ISSN Application No. 21803

Indian Journal of Mechanical and Thermal Engineering

Volume No. 7

Issue No. 3

September - December 2023

ENRICHED PUBLICATIONS PVT. LTD

S-9, IInd FLOOR, MLU POCKET,
MANISH ABHINAV PLAZA-II, ABOVE FEDERAL BANK,
PLOT NO-5, SECTOR-5, DWARKA, NEW DELHI, INDIA-110075,
PHONE: - + (91)-(11)-47026006

ISSN Application No. 21803

Indian Journal of Mechanical and Thermal Engineering

Aims and Scope

Indian Journal of Mechanical and Thermal Engineering is a peer-reviewed journal for the presentation of original contributions and the exchange of knowledge and experience on the sciences of heat transfer and thermodynamics, and contribute to the literature of engineering sciences on the national and international areas but also help the development of mechanical engineering. engineers and academicians from disciplines of power plant engineering, energy engineering, building services engineering, HVAC engineering, solar engineering, Wind engineering, Nano engineering, surface engineering, thin film technologies, and computer aided engineering will be expected to benefit from this journal's conclusions.

ISSN Application No. 21803

Indian Journal of Mechanical and Thermal Engineering

Managing Editor
Mr. Amit Prasad

Editorial Board Members

Dr. Mamta Sharma
Assistant Professor,
Department of Applied Physics,
University Institute of Engineering and Technology,
Panjab University, Chandigarh
mamta.phy85@gmail.com

Dr. G.P Govil
Northern India Institute of Technology
gpgovil@gmail.com

Dr. Atul Goyal
Lala Lajpat Rai Institute of Engineering and Technology,
Moga- Ferozepur, Punjab 142001
atulmech79@yahoo.com

ISSN Application No. 21803

Indian Journal of Mechanical and Thermal Engineering

(Volume No. 7, Issue No. 3, September - December 2023)

Contents

Sr. No.	Articles / Authors Name	Pg. No.
1	To Influence The Process Parameters of CNC Milling Machine using the Taguchi Method on Hot Die Steel H-13 - *Parveen Kumar, Deepak Choudhary*	129 - 134
2	(6061) by using Different Tool Shapes in Friction Stir Welding - *Yadvinder Singh, I. C. Ramola*	135 - 142
3	Stabilized Mixed Finite Element Analysis for Heat Flow Inside Industrial Furnaces with Horizontal Burners - *Jaafar Albadr, Mofdi El-amrani, Mohammed Seaid, Jon Trevelyan*	143 - 152
4	Prediction of Angular Distortion in Mig Welded Stainless Steel 409l Plates by Mathematical Modeling - *Rishabh Narang, Vibhu Maheshwari, Pradeep Khanna*	153 - 160
5	Comparative Studies in Minimizing the Corrosion Behavior of AA7075 through Advancedcoating Techniques - *S. Premkumar, G. Naveen Subramanian*	161 - 167

To Influence the Process Parameters of CNC Milling Machine using the Taguchi Method on Hot Die Steel H-13

Parveen Kumar*, Deepak Choudhary**

*Scholar (MED)/ Yamuna Institute of Engg. & Technology Jagadhri,Yamunanagar/Haryana

**Asstt. Proff. (MED) / Yamuna Institute of Engg. & Technology Jagadhri,Yamunanagar/Haryana

A B S T R A C T

In order to build up a bridge between quality and productivity, the present study highlights optimization of CNC milling process parameters to provide high material removal rate (MRR). The material removal rate (MRR) have been identified directly related to productivity .In this paper Taguchi method is applied to find out the influence of various machining parameters like Spindle speed (SS) , feed rate (FR), depth of cut (DOC) on the quality characterstic Material removal rate (MRR) using Hot Die Steel H-13 work piece on Vertical CNC Milling machine. A L9 Orthogonal array is used to carry out the various experimental data in Mini Tab 15. Results obtained are plotted by Main effects MRR v/s SS, FR,DOC . The experimental results shows that in order to increase the productivity the quality characteristic MRR is optimised by the increase of control parameter Spindle speed & Depth of cut.

In this study, it was observed that, the order of significance of the main variables is as Spindle speed , depth of cut ,feed rate.

Keywords: Hot Die Steel H-13, Vertical Milling Machine, Taguchi Method.

INTODUCTION:

Robust design is an engineering methodology for obtaining product and process conditions, which are minimally sensitive to the various causes of variation to produce high-quality product with low development and manufacturing costs. Various optimizations' techniques are being used by technologists and researchers to optimize the process. Engineering optimization provides engineers with a rigorous, systematic method for rapidly zeroing in on the most innovative, cost effective solutions to some of today's most challenging engineering problems; optimization is a powerful tool of the trade for engineers in virtually every discipline (Rao 2001). Taguchi's parameter design is an important tool for robust design. It offers a simple and systematic approach to optimize design performance, quality and cost.

MATERIAL & METHOD:

STEPS: TAGUCHI

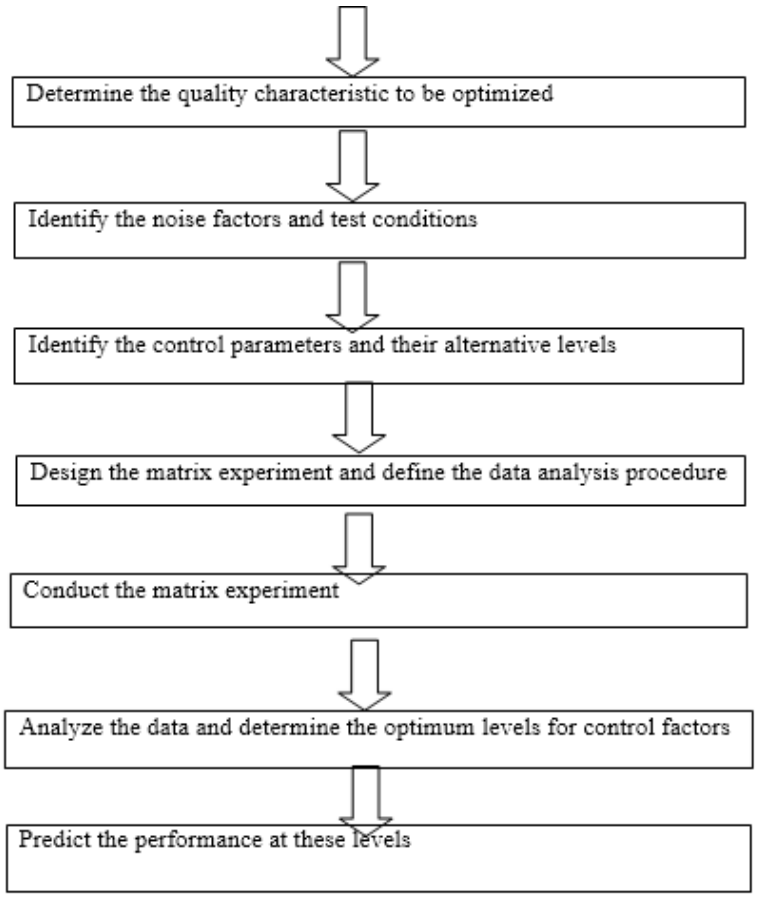

MATERIAL DESCRIPTION:

Sr. no.	Product description	Size of the material(mm^3)	Weight of the material (Kg)	Main Constituent of Hot Die Steel H13	Tool Material
1	Hot Die steel H13 Alloy steel/die steel/carbon steel/tool steel	140X100X25	3.3	Iron	Solid Carbide

Side view of H-13 material

EXPERIMENTAL WORK:

Control Parameters & their alternative levels by the use of L9 Orthogonal array data obtained from Mini

Tab 15 are Tabulated as:

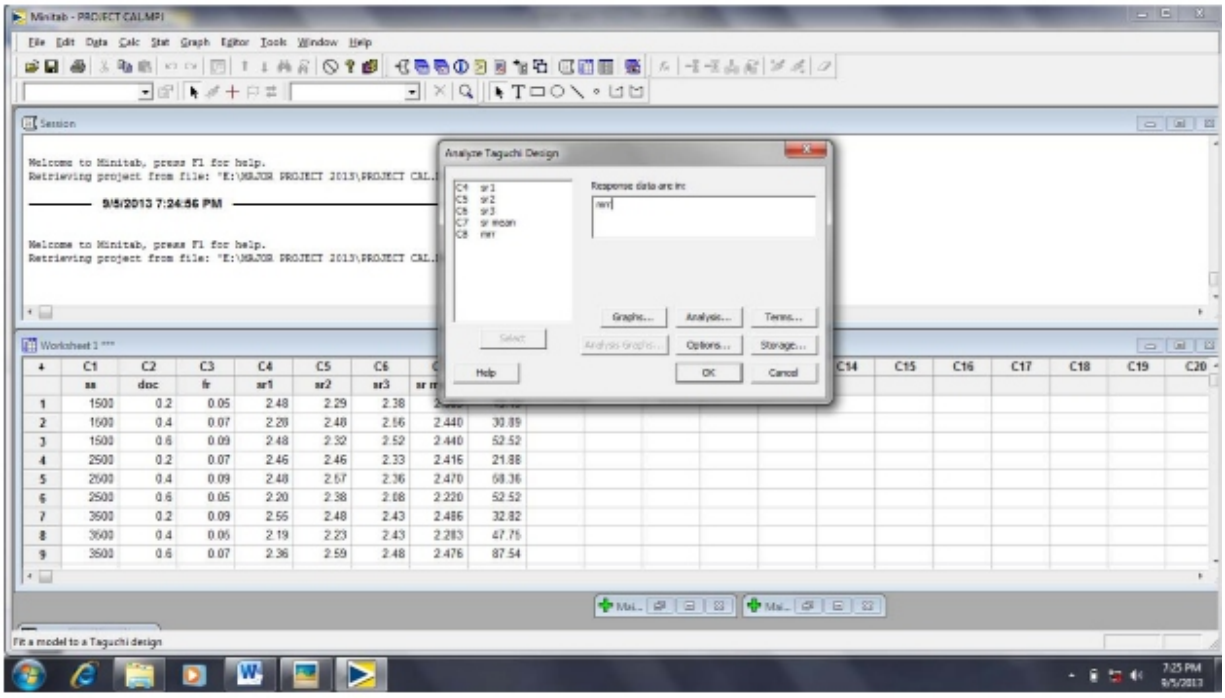

SR. NO.	SPINDLE SPEED(rpm)	DEPTH OF CUT (mm)	FEED RATE (mm/teeth)
1	1500	0.2	0.05
2	1500	0.4	0.07
3	1500	0.6	0.09
4	2500	0.2	0.07
5	2500	0.4	0.09
6	2500	0.6	0.05
7	3500	0.2	0.09
8	3500	0.4	0.05
9	3500	0.6	0.07

Different level of input factor

Surface Grinding of H-13

Operations on CNC Milling Machine

RESULTS & DISCUSSION:

SPINDLE SPEED(rpm)	DEPTH OF CUT(mm)	FEED RATE (mm/teeth)	MACHINING TIME(Sec)	MRR in mm^3sec
1500	0.2	0.05	20	13.13
1500	0.4	0.07	17	30.89
1500	0.6	0.09	15	52.52
2500	0.2	0.07	12	21.88
2500	0.4	0.09	9	58.36
2500	0.6	0.05	15	52.52
3500	0.2	0.09	8	32.82
3500	0.4	0.05	11	47.75
3500	0.6	0.07	9	87.54

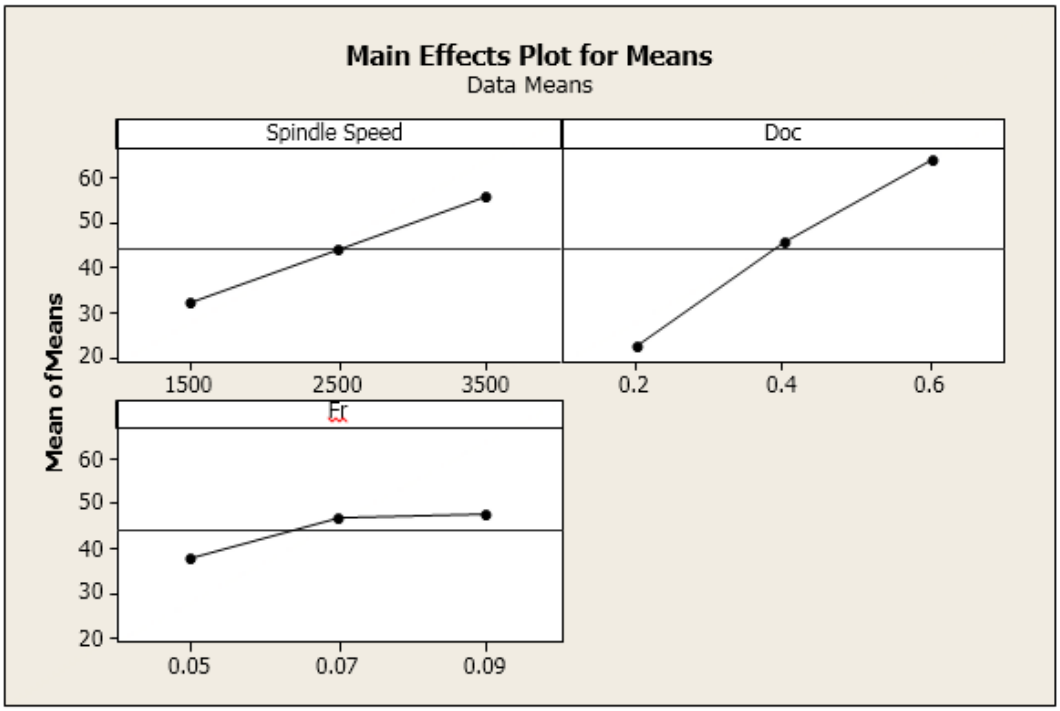

Main Effects (MRR)

As there are numbers of parameters which affect the material removal rate in Vertical CNC milling machine . According to present work conditions mainly three cutting parameters named Spindle speed, Depth of Cut , Feed rate may be selected and optimize the Material Removal rate using the DOE in Minitab sof tware package.

In this case the experimental results demonstrate that the Spindle speed and DOC are the main parameters that influence the MRR of Vertical CNC milling machine. The graph MRR v/s Spindle speed, depth of cut shows that as the MRR is directly proportional to spindle speed & DOC.

The optimum value of MRR is 87.54 mm3/sec.obtained at Spindle speed 3500 r.p.m. & 0.6 mm of feed rate. So as we increase the Spindle speed & Depth of cut the MRR also increase.

REFERENCE:

1. *Shah,B Ishan and Gawande,R. Kishore, " Optimization of Cutting tool life on CNC Milling Machine Through Design of Experiments –A Suitable Approach –An overview", Inernational Journal of Engineeering and Advanced Technology, ISSN: 2249-8958, Volume-1,Issue -4 April 2012.*
2. *Kumar Umesh et. All, "Experimental Investigation of Machining parameters of Vertical CNC Milling Machine on Hot Die Steel (H-13)", International Journal of Engineering Research & Indu. Appls, ISSN 0974-1518, Vol 5, No. III (August 2012) pp.69-80.*
3. *Kaya, Bulent, Oysu , Cuneyt , Ertunc ,M . (2011), "Force-torque based on-line tool wear estimation system for CNC milling of Inconel 718 using neural networks", advace in engginearing software 42, 76-84.*
4. *Rashid, M.F.F. and Abdul lani, M.R. (2010), "surface roughness prediction for CNC Milling process using artificial neural network", Volume 3, Number 1.*
5. *Moshat Sanjit, Datta Saurav et. all, " Optimization of CNC milling process parameters using PCA-based Taguchi method" , Journal of Engineering Science and Technology, Vol. 2, No. 1, 2010,pp. 92-102.*
6. *K.P. Patel, " Experimental Analysis on Surface Roughness of CNC End Milling Process using Taguchi Method" , International Journal of Engineering Science and Technology.*

(6061) by using Different Tool Shapes in Friction Stir Welding

Yadvinder Singh*, I. C. Ramola**

*Student/Ambala College of Engg. And Applied Research (Mithapur)/MED/KUK/Haryana

**Assistant Professor/ Ambala College of Engg. And Applied Research, Mithapur,/Med/Kuk/Haryana

ABSTRACT

In this experimental work, an extensive investigation had been carried out on Al Alloy (AA6061) grade aluminum alloy plates. This material is taken under investigation due its popularity in aircraft. The material of weld tool used High Carbon Steel. The tool material is used high carbon steel due to its low wear rate. Hence an attempt has been made to study the effect of influence of tool shape on the mechanical properties (tensile strength) of (AA6061) in single and double sided friction stir welds in this project. In this work the speed of tool rotation were taken as 3080 rpm, transverse speed as 30mm/min. and tool tilt angle was taken as 20. In both single and double pass, the highest tensile strength of the joints was obtained by using the square pin profile tool. The square pin profiles tool is best and tensile strength significantly decreases for, cylindrical, triangular and threaded pin profile tool due to defect formation. In double sided weld, the joints fabricated by cylindrical pin profiled tool showing almost matching tensile properties to that of square pin tool profile.

Keywords: Al-Alloy (6061), High Carbon Steel Tool, Mechanical Property (Tensile)

Friction stir welding (FSW), a solid-state welding process was invented and experimentally proven by Wayne Thomas and a team of his colleagues at the Welding Institute UK and patented by the TWI in 1991, emerged as a welding technique to be used in high-strength alloys that are difficult to join with conventional technique . The process was developed initially for aluminum alloys, but since then FSW was found suitable for joining a large number of materials. In aeronautics, for instance, riveting is the preferred manufacturing process for aircraft fuselage structures; nevertheless, In FSW process, a non-consumable rotating tool, consisting of a shoulder and profiled probe or pin, is forced down into the joint line under conditions where the frictional heating is sufficient to raise the temperature of the material to the range where it is plastically deformed as shown in figure. In friction stir welding (FSW) a rotating cylindrical, shouldered tool with a profiled probe penetrates into the material until the tool shoulder contacts with the upper surface of the plates, which are butted together as shown in

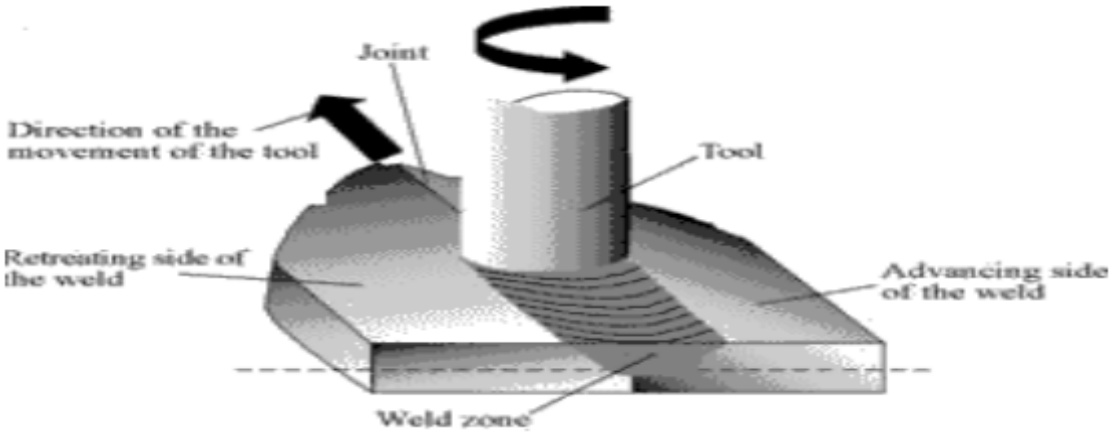

The parts have to be clamped on to a backing bar in a manner that prevents the abutting joint faces from being forced apart. Frictional heat is generated between the wear resistant welding tool and the material of the work pieces. This heat causes the later to soften without reaching the melting point and allows traversing of the tool along the weld line. In aluminum alloys, the mechanical properties of friction stir welds are usually better than those produced by conventional gas metal arc welding. Most of the work in friction stir welding has been done on aluminum alloys, where the mechanical properties were near those of the base plate. A number of potential advantages of FSW over conventional fusion-welding processes have been identified Good mechanical properties in the as welded condition. Improved safety due to the absence of toxic fumes or the spatter of molten material. No filler materials are required.

COMPOSITION OF AL ALLOY6061

The base material (BM) used in this investigation is aluminium alloy (AA6061). The chemical composition of the material is given in Chemical composition of aluminium alloy (AA6061)

Material	Mg	Cu	Mn	Si	Fe	Cr	Al
AA6061	0.8-1.2 %	0.15-0.40%	0-0.15%	0.40-0.80%	0-0.7%	0.04-0.35%	Remainder

TOOL USED FOR SET UP

Diameter of tool head used 17 mm.

Dimensions of welding tools are given below length of tool – 50 mm, head diameter- 17 mm

For Single sided friction stir welding

1. Straight Cylindrical (SC) – pin diameter-5mm and pin length – 6 mm
2. Square (SQ)- pin dimensions –(5x5)mm , diagonal 7 mm and pin length – 6 mm
3. Cylindrical Threaded (TH) – pin diameter 6mm , pitch of thread- 0.7 mm, pin length- 6 mm
4. Triangular (TR) – diagonal – 5mm , pin length- 6 mm

Similarly four shapes of tools being used for double sided FSW dimensions are given below

1. Straight Cylindrical (SC) – pin diameter-5mm and pin length – 3 mm
2. Square (SQ)- pin dimensions – (5x5)mm , diagonal -7 mm and pin length – 3 mm
3. Cylindrical Threaded (TH) – pin diameter 6mm , pitch of thread- 0.7 mm, pin length- 3mm
4. Triangular (TR) – diagonal – 5mm , pin length- 3 mm

All tools were machined on the basis that the maximum shank diameter of tool should be 17 mm.

PROCEDURE FOR FRICTION STIR WELDING

First of all seventeen pieces having size 100x50x6mm of AA6061 material are prepared for friction stir welding purpose. For this firstly AA6061material blank is pressed in a press to make it straight and stress free. After that from this material blank, thirteen plates of size 100x50x6mm are cut on shaper machine as shown in figure. After cutting plates of proper size, then the edges of these plates are made straight by passing cutting tool at angle 90° simultaneously on all the pieces. Then these plates are made burr free by filing so that when two plates are kept in fixture simultaneously for friction welding, then there should not be any gap present between two pieces in order to make better samples for friction welding. In this work the tool rotation speed kept constant at 3080 rpm, transverse speed was 30mm/min. and tool tilt angle was taken 20.Tool tilt angle given to provide required pressure in the welding.

TENSILE TESTING

Tensile testing, also known as tension testing, is a fundamental material science test in which a sample is subjected to a controlled tension until failure. The results from the test are commonly used to select a material for an application, for quality control, and to predict how a material will react under other types of forces. Properties that are directly measured via a tensile test are ultimate tensile strength, maximum elongation and reduction in area. A tensile specimen is a standardized sample cross-section. It has two shoulders and a gauge (section) in between. The shoulders are large so they can be readily gripped, whereas the gauge section has a smaller cross- section so that the deformation and failure can occur in this area.

Steps involved before the test were

1. Make gauge marks on the specimen.
2. Measure the initial gauge length.
3. Load scale to deform and fracture the specimen taken is Kgf on UTM.

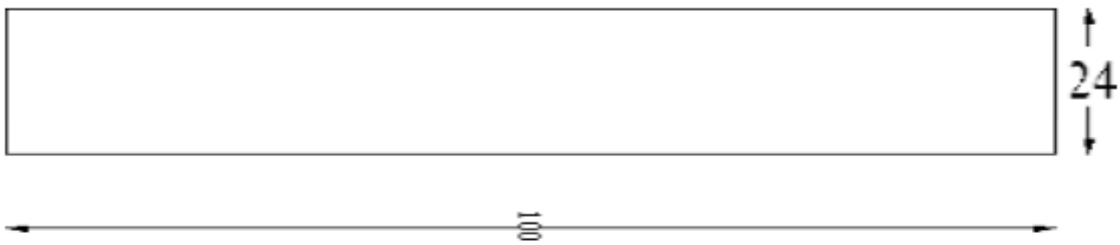

Specimen's Dimensions

Before testing welded specimen (single and double sided) were assigned number as S1to S4 for single pass specimen and S5 to S8 for double pass specimen.

Sr. No.	Specimen name	Type of weld pass	Tool shape
1	S1	Single	Square
2	S2	Single	Straight cylindrical
3	S3	Single	Cylindrical threaded
4	S4	Single	Triangular
5	S5	Double	Square
6	S6	Double	Straight cylindrical
7	S7	Double	Cylindrical threaded
8	S8	Double	Triangular
9	S9	Base metal	-

Steps followed during the tensile test.

1. Record the maximum load.
2. Conduct the test until fracture.

After the test Measure the final gage length and calculate Elongation. The length has been measured according to the gage marking. Mechanical properties which had been tested are

a. Ultimate tensile strength
b. Percentage of elongation
c. By finding UTS, joint efficiency of samples

RESULTS AND DISCUSSIONS

The welded specimens were put under tensile testing and the values of ultimate tensile strength, percentage elongation and joint efficiency were noted. The results of tensile loading of the base metal and welded specimens in single and double pass are shown in Table 1, Table 2 and Table 3 respectively. The variation of ultimate tensile strength, percentage elongation and joint efficiency are shown in Graphs 1- 3 respectively.

Formulae used for mechanical testing are given below

Stress :- Load/Area All load values we got from testing are in Kgf. For conversion of kgf into N/mm2:-1 kgf :- 9.8 N/mm2

1. Percentage Elongation :- (Final length – initial length)/100
2. Joint Efficiency :- UTS of welded specimen/UTS of base metal

On the basis of above formulae, we can make the Table for tensile testing of specimen in single and double pass.

TABLE 1 Tensile Test Results of Base Metal

Specimen No.		Ultimate Tensile Strength		Percentage Elongation	
	Area(in mm^2)	Load (kgf)	Stress (N/mm^2)	Elongated Length (mm)	% Elongation
S9	87	1150	130	56.5	11.5

TABLE 2 Tensile testing Results of welded specimen in single pass

Specimen No.		Ultimate Tensile Strength		Percentage Elongation		Joint Efficiency (%)
	Area(in mm^2	Load (kgf)	Stress (N/mm^2)	Elongated Length (mm)	% Elongation	
S1	144	1248	85	55.3	9.5	65.3
S2	142.8	1208	83	54.25	7.8	63.8
S3	144	1104	75	53	5.6	57.6
S4	142.2	1148	79	54.1	7.5	60.7

TABLE 3 Tensile testing Results of welded specimen in double pass

Specimen No.		Ultimate Tensile Strength		Percentage Elongation		Joint Efficiency (%)
	Area(in mm^2	Load (kgf`)	Stress (N/mm^2)	Elongated Length (mm)	% Elongation	
S5	139.2	1292	91	55.45	9.8	70
S6	144	1280	87	55.38	9.7	66.9
S7	44.6	1132	77	54.2	7.7	59.23
S8	143.1	1208	83	55.2	9.4	63.8

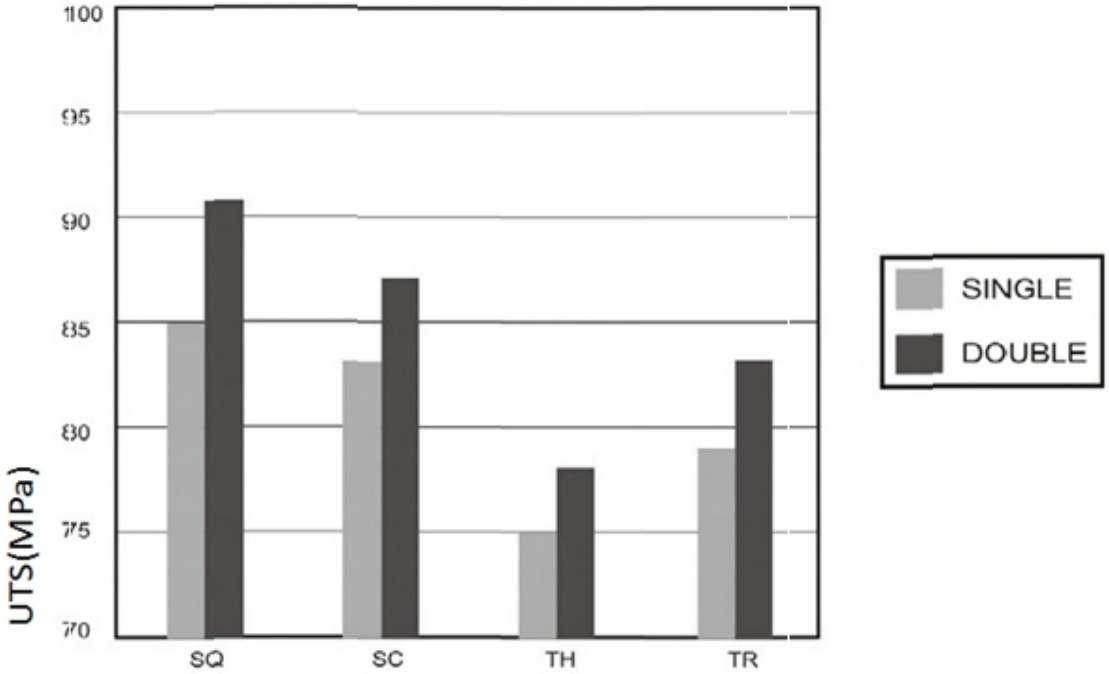

Graph 1 Variation of Ultimate Tensile Strength

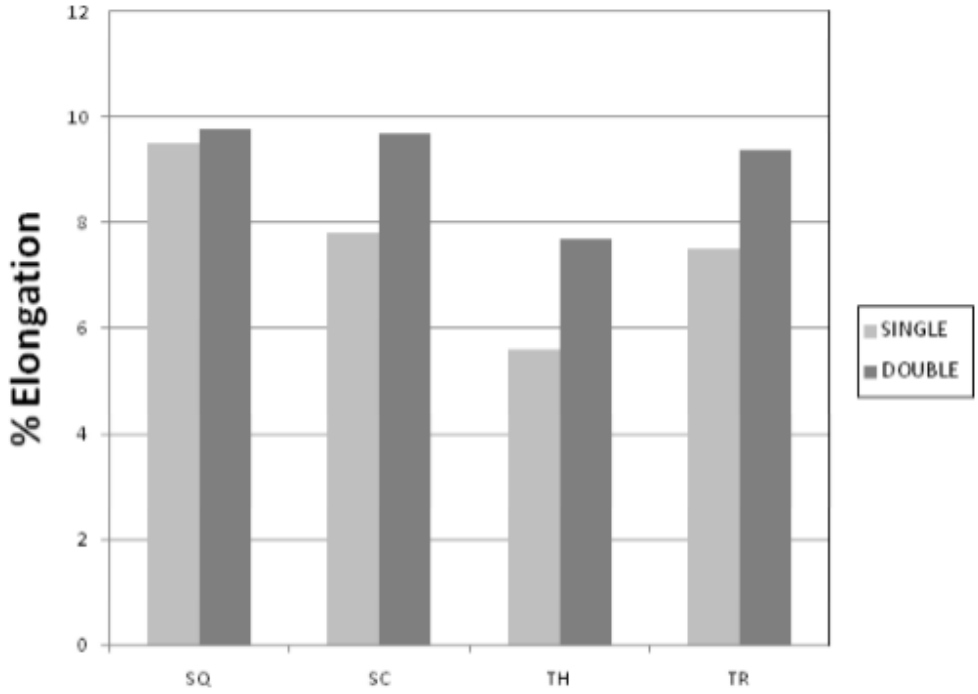

Graph 2 Variation of Percentage Elongation

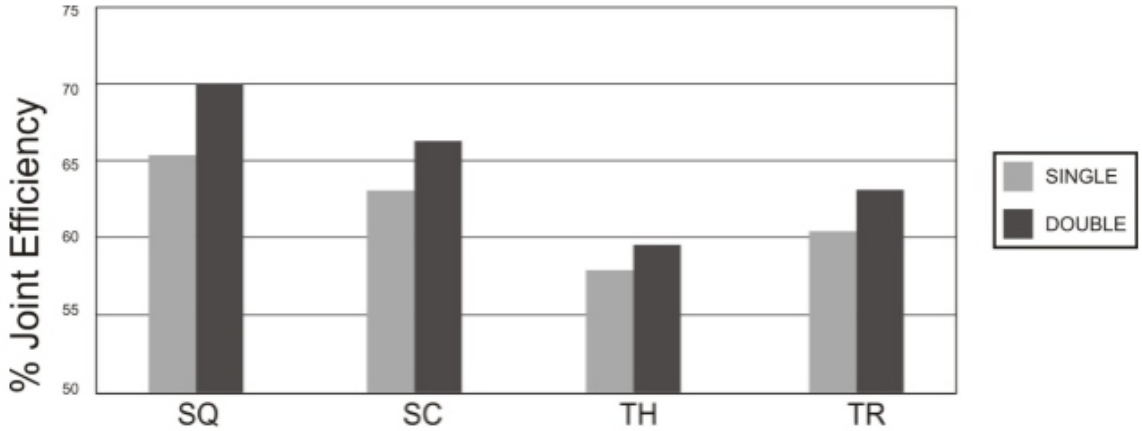

Graph 3 Variation of Joint Efficiency

Tensile properties of FSW joints i.e. ultimate tensile strength, percentage elongation and joint efficiency were evaluated. From the graphs, it can be seen that the tool profile and passing of tool in full depth in single pass and half in double pass are having influence on tensile properties of the FSW joints. In both single and double pass, the highest tensile strength of the joints was obtained by using the square pin profile tool. The square pin profiles tool is best and tensile strength significantly decreases for cylindrical, triangular and threaded pin profile tool . Square tool pin profile tool exhibited superior tensile properties compared to other joints,. Similarly, the joints fabricated by triangular pin profiled tool are also showing almost matching tensile properties to that of square tool profile in double sided weld. The joints fabricated by single pass have shown lower tensile strength and lower percentage of elongation compared to the joints fabricated by double pass and this trend is common for all the tool profiles. The joints fabricated by threaded pin profile tool in single sided weld shown inferior joint efficiency.

CONCLUSIONS

In this investigation an attempt has been made to study the effect of tool pin profile (square, straight cylindrical, threaded and triangular) on the formation of friction stir processing zone in a single and sequential double sided friction stir weld in Al Alloy (Aa6061). From this investigation, the following important conclusions are derived:

(I) The joints fabricated by double pass weld have shown higher ultimate tensile strength and also higher percentage of elongation as compared to the joints fabricated by single pass for all the tool profiles.

(ii) Square pin tool having superior joint efficiency among all tool profiles.

(iii) The joints fabricated by threaded pin profile tool in single sided weld shown inferior joint efficiency due to crack formation.

(iv) The joints fabricated by double pass weld have shown higher ductility as compare to the joints fabricated by single pass for all tool shapes.

REFERENCES

1. *Fujii ,Hidetoshi., Cui ,Ling., Maeda, Masakatsu., Nogi, Kiyoshi., " Effect of tool shape on mechanical properties and microstructure of friction stir welded aluminum alloys", Materials Science and Engineering Journal A 419 (2006) pp 25–31*
2. *Ahmadi, H., Mostafa ,Arab, N.B., Ashenai ,Ghasemi F., Eslami, Farsani, R., "Influence of pin profile on quality of friction stir lap weld in carbon fibre reinforced polypropylene composit" international journal of machanics and applications, (2012) P-ISSN:2165-92*
3. *Rao, P.N., Manufacturing Technology, Second Edition, Tata McGraw Hill Edition, 2006*
4. *Kumar, K., V.,Kailas, Satish., & Srivatsan ,T.S., "Influence of Tool Geometry in Friction Stir Welding", Journal of Materials and Manufacturing Proceesses, 23 (2008) pp 188- 194*
5. *Sarvghad, Moghddam, M., Parvizi, R., Haddad,Sabzevar,M., Davoodi, A., "Microstructure and Mechanical properties of friction stir welded Cu 30 Zn brass alloy at various feed speed : influence of stir bend" Material and design 32 (2011) 2749-2755.*
6. *Ren, S.R., Ma, Z.Y., Chen, L.Q., "Effect of welding parameters on tensile properties and fracture behavior of friction stir welded Al-Mg-Si alloy", Scripta Matererialia 56 (2007) pp 69-72.*
7. *Rajakumar, S., Balasubramanian, V., "Multi-Response optimization of Friction-Stir- Welded AA1100 Aluminum Alloy Joints", Journal of Material Engineering and Performance 21(2012) pp 809-822.*
8. *Payganch, G.H., Mostafa, N.B., Dadgar, Asl ,Y., Ghasemi, F.A., Saeidi ,Boroujeni, M., "Effects of friction stir welding process parameter on appearance and strength of polypropylene composite welds" international journal of the physical sciences vol.6(19) (2011) pp 4595-4601*
9. *Barcellona, A., Buffa, G., Fratini, L., Palmeri, D., "Microstructural phenomena occurring in friction stir welding of aluminum alloys", Journal of Materials Processing Technology ,177 (2006) pp 340-343.*
10. *Fujii ,Hidetoshi. , Cui ,Ling., Tsuji ,Nobuhiro., Maedac, Masakatsu., Kazuhiro, Nakata. , Nogi Kiyoshi ,"Friction stir welding of carbon steels", Materials Scienc and Engineering Journal A 429 (2006) pp 50–57..*
11. *Mohanty, H.K., Mahapatra, M.M., Kumar, P., Biswas P., Mandal ,N.R., "Effect of tool shoulder and pin probe profile on friction stirred alluminium welds" journal of marine science and application ISSN :1002-2848/CN:61-1400/f (2012) pp 200-207*
12. *Jariyaboon, M., Davenport, A.J., A.J., Ambat R., Connolly B.J., Williams S.W., Price D.A., "The effect of welding parameters on the corrosion behavior of friction stir welded AA2024-T351" Corrosion Science 49 (2007) pp 877-909.*

Stabilized Mixed Finite Element Analysis for Heat Flow Inside Industrial Furnaces with Horizontal Burners

[1] Jaafar Albadr, [2] Mofdi El- Amrani, [3] Mohammed Seaid, [4] Jon Trevelyan

[1,3,4]School of Engineering and Computing Sciences, University of Durham, South Road DH1 3LE, UK

[2]Universidad Rey Juan Carlos, Depo, Mathematica Aplicada, 28933 Madrid, Spain

E-mail: [1]jaafar.n.albadr@durham.ac.uk

A B S T R A C T

We propose a stabilized mixed finite element approach for the numerical simulation of heat transfer inside industrial furnaces with horizontal burners. The emphasis in this study is on large furnaces used for glass processing at moderate temperatures. The governing equations consist of thermal incompressible Navier-Stokes equations subject to the Boussinesq approximation to account for the changes in density. The numerical solver is based on combining the modified technique of characteristics with a Galerkin finite element discretization of the equations in primitive variables. It can be interpreted as a fractional step method where the convective part and the Stokes/Boussinesq part are treated separately. This solver avoids projection techniques and does not require any special correction for the pressure. We verify the method for a furnace with a single side operation of burner and with both sides operation of burners installed on the walls of the furnace. The proposed stabilized finite element method has been found to be feasible and satisfactory.

Keywords - Heat Transfer inside Industrial Furnaces, Mixed Finite Element Method.

I. INTRODUCTION

Furnaces have been widely used in the industry for decades and many researchers have been carried out to improve their performance [1]. Numerical methods in CFD, computational fluid dynamic can be a tool for design and simulation of heat transfer in furnace including burners and moving structures. The emphasis in this work is to simulate heat transfer in a furnace used for glass processing by incorporating burners. As first stage of the work, we focus on simulation of coupled convective flow and heat transfer in the furnace without accounting for radiation, combustion and deformation of glass sheet. Most of FEMs, finite element methods fail to resolve these problems mainly due to thermal boundary layer and high Reynolds numbers. In order to stabilize this class of finite element, we propose a Galerkin-characteristic procedure for which the convective and diffusive parts in the governing equations are solved separately. This method is highly accurate and unconditionally stable. Numerical results are presented for three test examples namely a furnace with single burner on the right hand side wall, a single burner on the left hand side wall and operation of both burners (left and right sides). The main challenges in this process are keeping a required temperature distribution over the entire glass sheet inside the furnace; avoid the presence of cracks and wrong bending. Moreover, controlling the temperature over the surface of the glass sheet can be done by controlling time, operation, location and the number of the burners on the left and right walls of the furnace in order to ensure the desirable results and prevent overheating. However, too low temperature inside the furnace chamber can also lead to a negative impact on the fuel consumption and the bending (deformation) process [2]. Furthermore, mapping data technique is one of the problems which happen due to the presence of advection terms in the fluid governing equations which can result in nodes oscillations at high Reynolds numbers. To overcome with these challenges, this paper addresses certain strategies: first, a uniform mixed FEM to

solve the heat flow. Likewise, Incompressible Navier-Stokes equations are considered for fluid as the burners blow the fire in a large volume domain that makes the pressure variation small as compared with the absolute pressure. Finally, the variation of density is considered only in the buoyancy term. One of the challenges related to the numerical solution of Navier-Stokes equations is calculation of pressure. Pressure is not a thermodynamic variable; this is the reason why there is no equation for calculating the pressure. Mixed FEM is considered to avoid such challenge. Linear triangular elements (three nodes) are taken into consideration for the pressure and quadratic triangle elements (six nodes) are taken into account for the temperature and velocity. This technique allows us to solve Navier-Stokes equations instead of interpolating lower degrees function. Furthermore, treated the numerical solution of convection-diffusion problems has been done by splitting method to avoid problems created when the convection term is dominant. Splitting method is done by solving the convection term first then the diffusion term.

II. MATHEMATICAL MODELLING

Fig. 1 represents a schematic of the geometry of the furnace studied in this work which consist of two-dimensional cross sectional thermal convection current in a furnace (with horizontal burners).

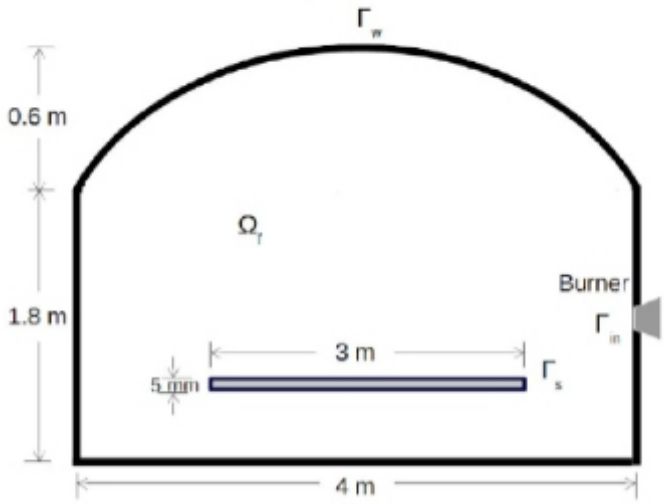

Fig.1. Cross sectional view of a furnace.

The furnace is essentially at room temperature which is 300K. Since the fluid is Newtonian, all the thermo physical characteristics are taken into account to be constant with the exception of density in the buoyancy term: it can be modeled sufficiently by the Boussinesq approximation [3], neglecting viscous dissipation and compression effects. Thickness of the structure sheet is very thin and heat radiation is not considered at this stage of the study. To reduce turbulence and oscillation generated from the convection term, low Reynolds number is considered. Combustion process is not considered as the combustion process takes place outside the investigated domain. Based on these considerations, the dimensionless incompressible Navier-Stokes are

$$\nabla \cdot \mathbf{u} = 0,$$

$$\frac{\mathbf{Du}}{\mathbf{Dt}} + \nabla p - \frac{1}{\mathrm{Re}} \nabla^2 \mathbf{u} = (T - \frac{1}{2})\mathbf{e}, \qquad (1)$$

$$\frac{DT}{Dt} - \frac{1}{\mathrm{PrRe}} \nabla^2 T = 0.$$

Where u(x,t) is the velocity field, T the temperature, p the pressure, Re the Reynolds number and Pr thePrandtl number. In (2), the material derivative of generic function ω is

$$\frac{D\omega}{Dt} = \frac{\partial \omega}{\partial t} + u \cdot \nabla \omega \qquad (2)$$

On the domain boundary $T = T_w \cup T_s \cup T_{in}$. The following conditions have been used.

$$\begin{aligned} u &= 0 && \text{on } \Gamma_w \cup \Gamma_s. \\ u &= u_{in} && \text{on } \Gamma_{in}. \\ T &= T_{in} && \text{on } \Gamma_{in}. \\ T &= T_b && \text{on } \Gamma_w. \\ n \cdot \nabla T &= 0 && \text{on } \Gamma_s. \\ -pn + \frac{1}{Re} n \cdot \nabla u &= 0 && \text{on } \Gamma_s. \end{aligned}$$

Initially, the flow is at rest with a room temperature T=300K. In all our simulations, Tb=300K, Tin=1000K and uin = -10m/s.

III. SOLUTION PROCEDURE

Since standard Galerkin discretization leads to the central difference approximation of differential operators, Galerkin approximations to the convection equations usually suffer instability problems. Among various approaches to improve stability, streamline upwind Petrov-Gealerkin, Taylor-Galerkin and characteristic-Galerkin schemes have gained some popularity. Before applying the spatial discretization, the characteristic-Galerkin scheme discretizes, the original equation in time along the characteristic curves. It can be implemented in the framework of standard Galerkin finite element formulation. In this section we briefly describe the ingredients of the numerical scheme used and for more details we refer to [4, 5, 6] and further references are cited there in.

We chose a time step δt and descritize the time domain into subintervals $[t_n, t_{n+1}]$ with $t_n = n\Delta t$ and n = 0, 1, …. We denote $w^n(x) = w(x,t_n)$ for any genetic function w, we also denote by $X(x, t_{n+1};t)$ the characteristic curves associated with the material derivative (2) which solve the following initial value problem

$$\begin{aligned} \frac{dX(x,t_{n+1};t)}{dt} &= u\,(X(x, t_{n+1}; t), \\ (x,t) &\in \Omega \times [t_n, t_{n+1}], \qquad (3) \\ X(x, t_{n+1}; t_{n+1}) &= x. \end{aligned}$$

Notice that $X(x, t_{n+1}; t) = (X(x, t_{n+1}; t), Y(x,t_{n+1};t))^T$ is the departure point and represents the position at time t of a particle that reaches the point $x = (x,y)^T$ at time t_{n+1}. Hence, for all $x \in \bar{\Omega} = \Omega \cup \partial\Omega$ and $t \in [t_n, t_{n+1}]$ the solution of (3) can be expressed as

$$X(x, t_{n+1}; t_n) = x - \int_{t_n}^{t_{n+1}} u\,(X(x, t_{n+1}; t), t)dt. \qquad (4)$$

Accurate estimation of the characteristic curves $X(x, t_{n+1}; t_n)$ is important to the overall accuracy of the characteristic-Galerkin approach. In this paper, the technique utilized was first proposed in [7] in the context of semi-Lagrangian schemes to integrate the weather prediction equations.

The discretization of the space domain Ω is proceeding as follows. Given h_O, $0 < h_O < 1$, let h be a partial discretization parameter such that $0 < h < h_O$. We generate a quasi-uniform partition $\Omega h \subset \Omega$ of small elements $\mathscr{J}_i$ that satisfy the following conditions:

(i) $\Omega = \cup_{j=1}^{Ne} \mathcal{J}_j$, where Ne is the number of elements of Ω_h.

(ii) If $\mathcal{J}_i$ and $\mathcal{J}_j$ are two different elements of Ω_h, then,

$$\mathcal{J}_i \cap \mathcal{J}_j = \begin{cases} P_{ij}, \text{ a mesh point, or} \\ \Gamma_{ij}, \text{ a common side, or} \\ \emptyset, \text{ empty set.} \end{cases}$$

(iii) There exists a positive constant k such that for all j ∈ {1, ….., Ne}, j > k (h hj j ≤ h), where dj is the diameter of the circle inscribed in $\mathcal{J}$j and hj is the largest side of $\mathcal{J}$j.

The conforming finite element spaces for velocity- temperature and pressure that we use are Taylor-Hood finite elements Pm / Pm-1 i.e., polynomial of degree m ≥ 2 for {u, v, T} and polynomial of degree m – 1 for p, respectively. An illustration is depicted in Fig. 2 for triangular mesh. It is known that for such elements the discrete velocity-temperature and pressure fields satisfy the inf-sup condition. These elements can be defined as

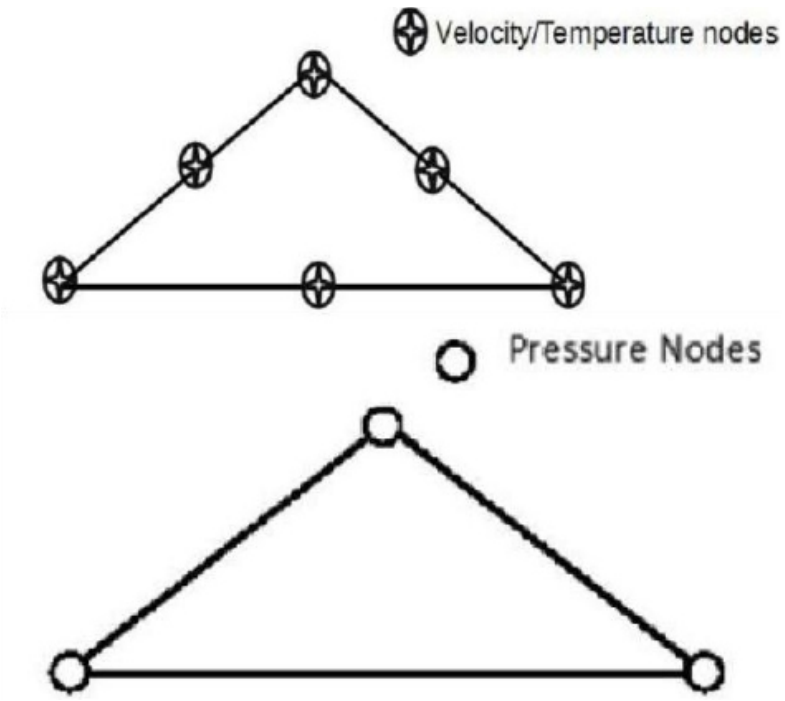

Fig.2. definition of Taylor-Hood finite element.

$V_h = \{ v_h \in C0(\Omega) : v_h | \mathcal{J}$
$)_h = \{ q_h \in C0(\Omega) : q_h | \mathcal{J}$
$\in S(\mathcal{J}_j), \forall \mathcal{J}_j \in \Omega_h \}$,
$\in S(\mathcal{J}_j), \forall \mathcal{J}_j \in \Omega_h \}$.

Where C0 (Ω) denotes the space of continuous and bounded functions in Ω, $S(\mathcal{J}_j)$ and $R(\mathcal{J}_j)$ are polynomial spaces defined in $\mathcal{J}_j$ as $S(\mathcal{J}_j)$ = Pm ($\mathcal{J}_j$) for simplexes, $S(\mathcal{J}_j)$ =)m($\mathcal{J}_j$) for quadrilaterals, $R(\mathcal{J}_j) = P_{m-1}(\mathcal{J}_j)$ for simplexes and $R(\mathcal{J}_j) =)_{m-1}(\mathcal{J}_j)$ for quadrilaterals. Hence, we formulate the finite element solutions to $u^n(x)$, $v^n(x)$, $T^n(x)$ and $p^n(x)$ as

$$u_h^n = \sum_{j=1}^{M} U_j^n \, \phi_j, \qquad v_h^n = \sum_{j=1}^{M} V_j^n \, \phi_j,$$

$$T_h^n = \sum_{j=1}^{M} \Lambda_j^n \, \phi_j, \; p^n = \sum_{h}^{N} P_j^n \, \psi_j, \qquad (5)$$

where M and N are respectively, the number of velocity-temperature and pressure mesh points in the partition Ω_h. The functions U_j^n, V_j^n, Λn and P_n are the corresponding nodal values of $u_n(x_h)$, $v_n(x_h)$, $Tn(x_h)$ and $p_j^n(x_h)$, respectively. They are defined as $U_h n = u_n(x_j h)$, $V_j n = v_n(x_j)$, $\Lambda n = T_n(x_j)$, and $P_n = p_n(y_j)$ where $\{x_j\}M_{j=1}$ and $\{y_j\}M_{j=1}$ are the set of velocity- temperature and pressure mesh points in the partition Ωh, respectively, so that $N < M$ and $\{y1,\ldots,yN\} \subset \{x1,\ldots,xM\}$. In (5), $\{\ \ j\}^M_{j=1}$ and $\{\psi\}^N_{j=1}$ are the set of global nodal basis functions of V_h and S_h, respectively, characterized by the property $\phi_i(x_j) = \delta_{ij}$ and $\psi_i(y_j) = \delta_{ij}$ with δ_{ij} denoting the Kronecker symbol.

Assuming that, for all j = 1, …, M, the pairs $(X_{hj}^n, \mathcal{J}_j)$ and the mesh point values $\{U_j^n, V_j^n, \Lambda_j^n\}$ are known, we compute the values $\{\acute{U}_i^n, \tilde{V}_i^n, \breve{\Lambda}_i^n\}$ as

$$\acute{U}_j^n := u_h^n(\mathbf{X}_{hj}^n) = \sum_{k=1}^{M} U_k \phi_k(\mathbf{X}_{hj}^n),$$

$$\tilde{V}_j^n := v_h^n(\mathbf{X}_{hj}^n) = \sum_{k=1}^{M} V_k \phi_k(\mathbf{X}_{hj}^n), \qquad (6)$$

$$\breve{\Lambda}_j^n := T_h^n(\mathbf{X}_{hj}^n) = \sum_{k=1}^{M} \Lambda_k \phi_k(\mathbf{X}_{hj}^n).$$

Then, the solution $\{\tilde{u}_h^n(x), \tilde{v}_h^n(x), \breve{T}_h^n(x)\}$ at the characteristic feet is obtained by

$$\tilde{u}_h^n(\mathbf{x}) = \sum_{j=1}^{M} \acute{U}_j^n \phi_j(\mathbf{x}),$$

$$\tilde{v}_h^n(\mathbf{x}) = \sum_{j=1}^{M} \tilde{V}_j^n \phi_j(\mathbf{x}), \qquad (7)$$

$$\breve{T}_h^n(\mathbf{x}) = \sum_{j=1}^{M} \breve{\Lambda}_j^n \phi_j(\mathbf{x}).$$

We should mention that the convectional characteristic-Galerkin methods in [4, 5] evaluate $\tilde{u}n$, $\tilde{v}_h^n$ and $\breve{T}_h^n$ using the L2- projection on the space of the velocity-temperature Vh. In many applications, the evaluation of integrals in the L2 – projection is difficult and computationally very demanding.

We consider a projection-type procedure to solve the Stokes/Boussinesq problem, compare [8] for similar method. Given $\{p^n, u^n, v^n, T^n\}$, we compute the solution $\{p^{n+1}, u^{n+1}, v^{n+1}, T^{n+1}\}$ as follows:

1. Solve for T^{n+1}

$$\frac{T^{n+1} - \breve{T}^n}{\Delta t} - \frac{1}{PrRe} \nabla^2 T^{n+1} = 0. \qquad (8)$$

2. Solve for $\bar{u}^{n+1}$

$$\frac{\bar{u}^{n+1} - \tilde{u}^n}{\Delta t} + \nabla p^n - \frac{1}{Re} \nabla^2 \bar{u}^{n+1} = (T^{n+1} - \frac{1}{2})\, e. \qquad (9)$$

3. Solve for $\dot{p}$

$$\nabla^2 \dot{p} - \frac{1}{\Delta t} \nabla \cdot \bar{u}^{n+1}. \qquad (10)$$

4. Solve for $\mathbf{u}^{n+1}$

$$\frac{\mathbf{u}^{n+1} - \bar{u}^{n+1}}{\Delta t} + \nabla \dot{p} = 0. \qquad (11)$$

5. Update p^{n+1}

$$p^{n+1} = p^n + 2\dot{p}. \qquad (12)$$

Note that Poisson problem (10) is established by taking the divergence of equation (11) and utilizing the fact that $\nabla \cdot u = 0$. In the solution procedure, four linear systems have to be solved at each time step to update the solution $\{p_{n+1}, u_{n+1}, v_{n+1}, T_{n+1}\}$ from (8)-(12). To solve these linear systems in our method we have implemented a preconditioned conjugate gradient algorithm.

IV. PRELIMINARY RESULTS

A very fine mesh which contains twice the mesh refinement of D is taken as a reference for the operation of both burners on left and right sides of the furnace walls at a time t=10s and time step Δt=0.01 with Re=500 (see Table 1 and Fig. 3). A horizontal cross sectional study taken y = 0.8 m (nodes and elements) has been taken into account for the calculation of the error percentage and CPU time for the velocity, temperature and pressure results for the five different meshes.

Horizontal cross sectional study covers the behavior of the heat flow across the furnace along the glass sheet length. From these results, mesh C is taken into account for the study of operation under single burner from the wall on left side, under single burner from the wall on right side and under both burners from both sides as it has a considerable percentage of errors and CPU time. The governing equations are solved in Ωf as it is shown in Fig. 1. When the burner is firing, convection heat transfer plays an important role in the distribution of temperature inside the furnace. Initially the furnace is at room temperature of 300 K. On the walls Γw, the temperature is set to 300 K while the adiabatic boundary conditions are for Γs. For the burners, heat flow of 1000 K is injected with a velocity of 10 m/s and computational results are illustrated at three different time intervals of (10, 30 and 60) s respectively with a fixed Reynolds number of 500. The operation is firing using one burner on the right, on the left and both at the same time.

The upper row of Fig. 4 shows the temperature distributions inside a furnace with both burners firing from both sides using the mentioned density of elements at Re=500 for the three time intervals. The second row (in the middle) represents heat flow from the burner installed on the right side of the furnace wall at time (t=10, 30 and 60) s respectively. The third row illustrates the third application of firing using burner installed on the left furnace wall. When the burner blows fire across the geometry of the furnace chamber, it induces turbulence and motion. The forced convection heat transfer is the result of the interaction between the fixed fluid inside the furnace which is at room temperature and the moving stream of the fire. The movement of the heat flow is very interesting. Two vortices can be observed from streamlines flow.

Fig. 5 show the horizontal cross sectional view for temperature distribution at t=10 s (the upper Fig.), at t= 30 s and t=60 s for the middle and the lower Figs. respectively. Results show high temperature fluctuations at the operation under two sides' burners as compared with single side burner. This is due to the fact that the turbulent behavior which is the result from the temperature difference that occurs inside the domain is high due to fewer amounts of heat sources. However, the operation under the right burner has the least temperature cross sectional fluctuation as the heat tends to flow towards the ceiling and accumulating at the right hand side of the furnace as the convection heat transfer drives the flow toward that direction. Another reason behind the this disposal is Reynolds number. Reynolds number generates flow vortices, eddies and wakes make the flow unpredictable during the transfer of heat from the hot layers to the colder layers. Results utilizing these operations at time t=60 s showed more turbulence and more temperature distribution variation as the temperature difference between the hot and the cold fluids increases dramatically.

As a result two vertices occur which force the heat flow to move downward towards the structure sheet. The time record of the temperature capture the minimum temperature value of 300 K at the horizontal cross sectional study with t= 10 s. This behavior in both operations of the left and the right burners firing separately shows undesirable results as the hot air flows upward towards the roof curvature. Convection heat transfer draws the flow towards the right side of the furnace leaving a considerable part from the centre of the furnace. This kind of heat flow behavior took place due to the air inside the furnace is still at room temperature which initially drag the heat away from the structure and towards the sides of the furnace roof ceiling inner surface. It can be seen that the flow tends to float. However at a certain time, the flow starts circulating and tends to movie downward due to the movement of the large vertices generated from turbulence. Fig. 6 shows a horizontal cross sectional velocity at t=10 s (upper Fig.), t=30 s (middle Fig.) and t=60 s (lower Fig.) respectively. The reason behind this kind of behavior is that when the flow gets heated up it becomes lighter and that hot light layers of the flow tend to move upward leaving their position to other colder layers to move downwards due to gravity. This kind of fluid conductance is the source of generating vortices. Those undesirable reasons that make the flow accumulate at the roof curvature. It is clear that the heat flow distribution inside the furnace vary dramatically. To reduce it, furnace must be covered with heat. Remarkable effects have been acquired from the operation of dual burners on both sides. First, the flow starts moving upward and towards the ceiling as the whole roof of the furnace is covered with heat which makes the flow unable to move upward even when the fluid is less dense. However, vortices start generating and moving close to the structure upper surface on both sides of the furnace. Heat accumulating at the side is due to higher temperature difference that draws the flow towards the sides of structure sheet.

	No. of elements	No. of nodes for T, u	No. of nodes for p	L^1-error in T	L^1-error in u	L^1-error in p	CPU time (seconds)
Mesh A	12062	24554	6246	0.1162	0.4826	0.7811	434
Mesh B	24085	48831	12373	0.0483	0.1247	0.2559	937
Mesh C	**48084**	**97046**	**24481**	**0.0107**	**0.0492**	**0.0691**	**2097**
Mesh D	96310	193938	48814	0.0091	0.0348	0.0457	5547
Ref. Mesh	192478	386692	97107	—	—	—	34645

Table 1: Results for the given meshes at time = 10 s.

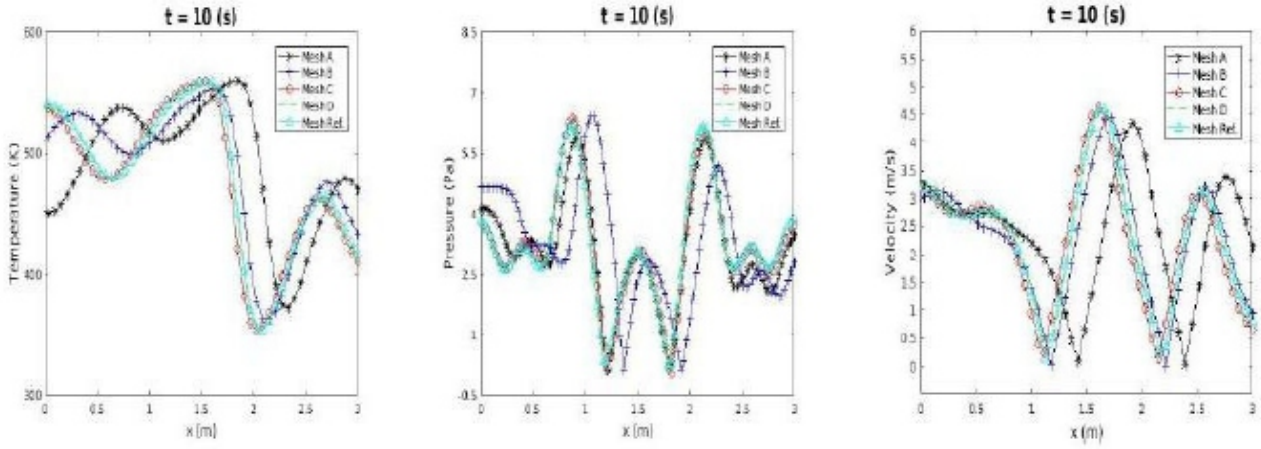

Fig.3. Horizontal cross-sections for temperature, velocity and pressure at time t = 10 s in the considered meshes.

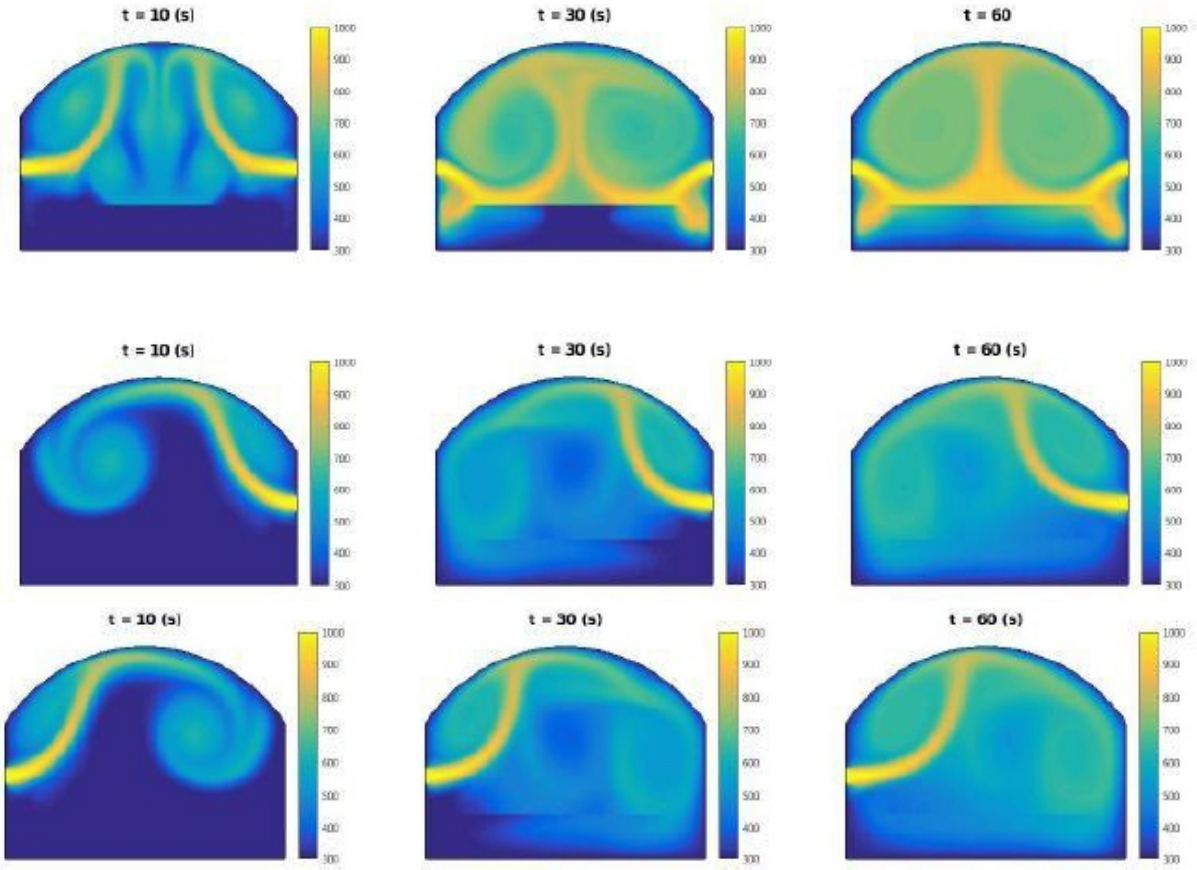

Fig.4. Distribution of temperature at three time intervals for dual operation of burners (on both sides) and for single operation of burner attached to left wall or attached to the right hand side.

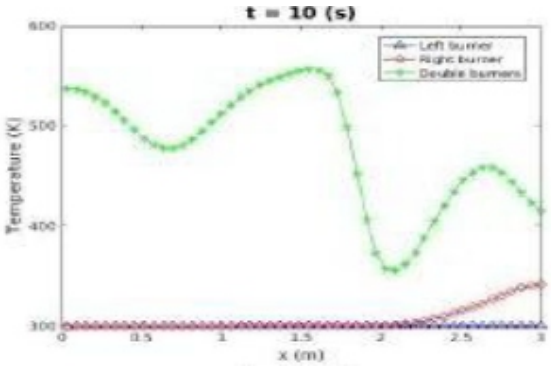

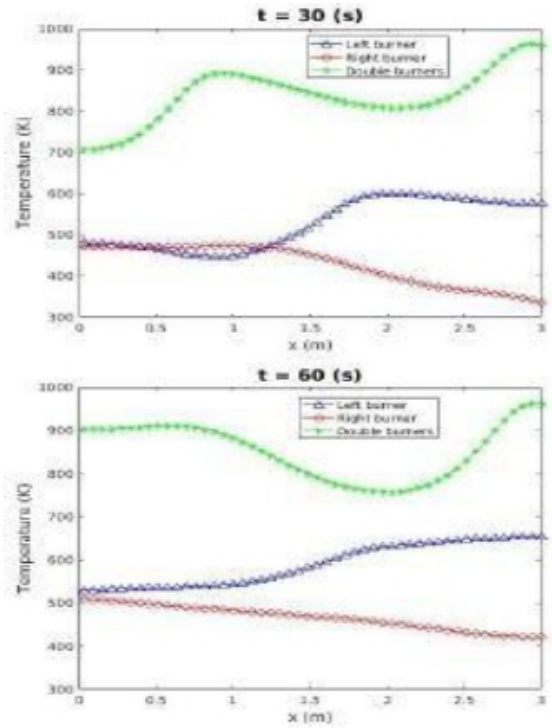

Fig.5. Temperature profile along x direction at three different times with Re=500.

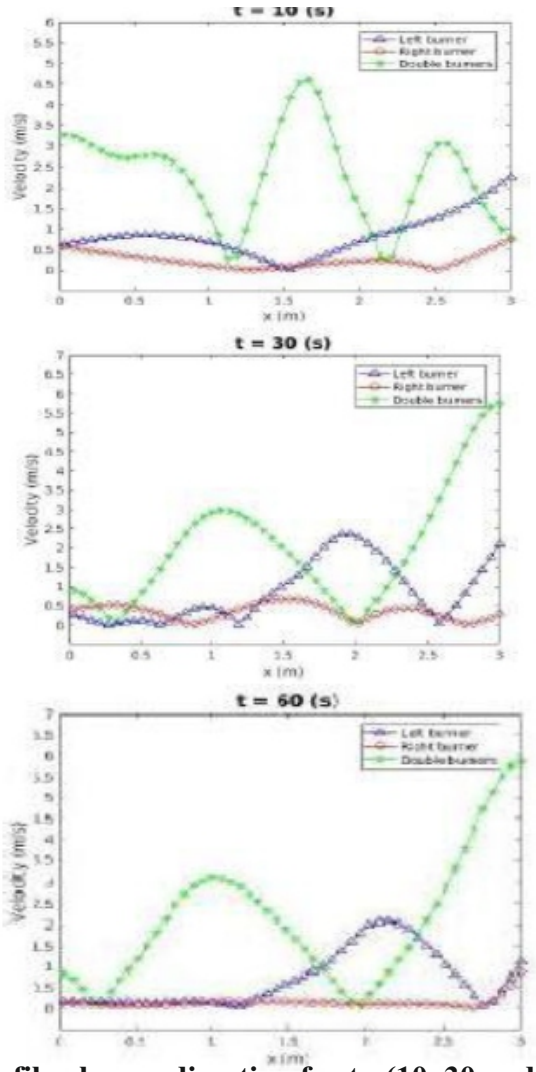

Fig.6. Velocity profile along x direction for t= (10, 30 and 60) s at Re=500.

CONCLUSIONS

In the present study, convective heat flow has been simulated and studied inside a furnace numerically utilizing a stabilized mixed finite element formulation for solving 2D incompressible non-denominational Navier-Stokes equations. The presented results show the behavior of the heat flow inside a furnace for three applications at the same Reynolds number. These results will enable us to: (i) control the desired temperature distribution over the glass sheet surface (ii) reduce the undesirable heat circulations and accumulations (iii) choose the required furnace dimensions (iv) increase furnace life time (v) reduce the fuel consumption and control number and operation of the burners which will help us in the next stage of study with the inclusion of radiation and thermo-elastodynamics coupling.

REFERENCES

[1] S. El-Behery, A. Hussien, and M. El-Shafie, "Performance evaluation of industrial glass furnace regeneration", Energy,vol.119,pp.1119–1130, 2017.

[2] Glass industry. [www.jumo.co.uk].

[3] Y. Jaluria, "Natural convection heat and mass transfer", Pergamon Ress, Oxford,1980.

[4] T. Douglas, and J. Russel, "Numerical methods for convection dominated diffusion problems based on combining the method of characteristics with finite elements or finite difference", SIAM Journal on Numerical Analysis,vol.19,pp.871–885, 1982.

[5] O. Pironneau, "On the transport-diffusion algorithm and its applications to the Navier-Stokes equations", Numerical Mathematics,vol.38,pp. 309-332, 1982.

[6] E. Suli, "Convergence and nonlinear stability of the Lagrange-Galerkin method for the Navier-Stokes equations", Numerical Mathematics,vol.53,pp.1025- 1039,1988.

[7] C. Temerton, and A. Staniforth, "An efficient two-time- level semi-Lagrangian semi-implicit integration scheme", Quartely Journal of Royal Meteological Society,vol. 113,pp.1025-1039,1987.

[8] M. El-Amrani, and M. Seaid, "Numerical simulation of natural and mixed convection flows by Galerkin-characteristic method", International Journal for Numerical Methods in Fluids,vol.53,pp.1819-1845,2006.

Prediction of Angular Distortion in Mig Welded Stainless Steel 409L Plates by Mathematical Modeling

[1] Rishabh Narang, [2] Vibhu Maheshwari, [3] Pradeep Khanna
[1]Student, Department of MPAE, NSUT, New Delhi-110078, India
[2]Student, Department of MPAE, NSUT, New Delhi-110078, India
[3]Associate Professor, Department of MPAE, NSUT, New Delhi-110078, India
E - Mail: [1]rishabh.narang102@gmail.com, [2]vibhumaheshwari25@gmail.com, [3]4.khanna@gmail.com

ABSTRACT

MIG welding is a preeminent joining process in which metalcoalesces by fusion and is extensively used in a variety of fabrication works. With the advancements in the field of industrial automation and availability of sophisticated power sources, it is now possible to achieve high production rates, repeatability, and weld quality. The significant amount of arc heat is used for the melting of faying surfaces which when followed by rapid cooling results in a number of micro and macro level changes in the resulting weld. One such physical change caused by the non-uniform rates of heating and cooling result in angular distortion of the weldment, which not only affects the aesthetics of the weld but also results in the misfit of the components with parent structure. It should be the endeavor of the weld engineer to keep this distortion to the minimum possible limit. The present work on SS409L aims to investigate the various impacts of welding input parameters on angular distortion. The experiments were perpetrated in a methodical manner and central composite face centered design(CCFD) technique was employed to generate the mathematical equation. The cumulative curve was determined by the welding parameters which were taken at five different levels. The model has been optimized by using response surface methodology (RSM). The research work carried out is expected to be useful for industry and for further advanced studies on the subject.

Keywords - Angular Distortion, Input Parameters, Mathematical Equation, MIG Welding, Stainless Steel

I. INRODUCTION

MIG weldingis a versatile welding process and is considered prominent due to many advantages offered by the process such as high reliability, high productivity, multi-position welding capabilityand ease of mechanization. The workpiece undergoes plastic deformation due to the tussle between contraction and expansion of different sections of weld interface thereby developing higher residual stresses. This leads to development of distortions like longitudinal, transverse and angular distortion. The outcome of uneven expansion along with non- uniform shrinkage of the weldmentis angular distortion as illustrated in figure 1 [1].

Fig. 1: Angular distortion

The factors affecting extent of angular distortion include width and depth of penetration of weldmentwith respect to thickness of plate, weld pass sequence, type of joint, input parameters and thermo- mechanical properties of the material [2].

In the fabrication industry angular distortion is a problem faced by engineers. By proving an initial angular compensation in the opposite direction, elimination of this perennial problem can be achieved. In order to obtain a weld without any angular distortion it is thereby vital to predict its correct measure precociously by using mathematical model. To examine the shape change deformation behavior of the component an in-depth analysis was performed. This led to development of suitable methods to control angular distortion. It is however strenuous to obtain analytical solutions for predicting angular distortion [3]. 409L is a low carbon variant of ferritic stainless steel.

Literature survey reveals that relatively less experimental work is available pertaining to this material so far. SS409L when exposed to high temperature shows excellent resistance capabilities towards oxidation. Its extra-low carbon ferritic structure makes it exemplary for typical applications which include automotive exhaust systems, heat exchangers, farm equipment components, etcetera [4,5].The composition of SS 409L is given in table – 1.

Element	C	Mn	P	S	Si	Cr	Ni	Cu	Mo	Ti	N(ppm)
Percentage (%)	0.0069	0.256	0.307	0.007	0.475	11.243	0.054	0.017	0.009	0.2033	51

Table - 1: Composition of Stainless Steel 409L (Provided by supplier) [6]

II. EXPERIMENTALARRANGEMENT

A mechanized welding carriage programmed to move in forward and reverse direction was used to conduct the experiments. The welding torch was positioned on a radial rotating arm which was orchestrated to move up-down and across the table. A gearbox arrangement with variable frequency drive and a driving motor were made use of to obtain smooth and step less control of carriage. The speed obtained of mechanized carriage varied from 0 - 50 cm/min. This unit ensured constant and uniform welding speed which resulted in consistent and reproducible welds. Filler wire made of SS 308L with 1.2mm diameter and a DC power source with flat V-I characteristics of 400 ampere rated capacity was employed, as illustrated in figure 2 below [7].

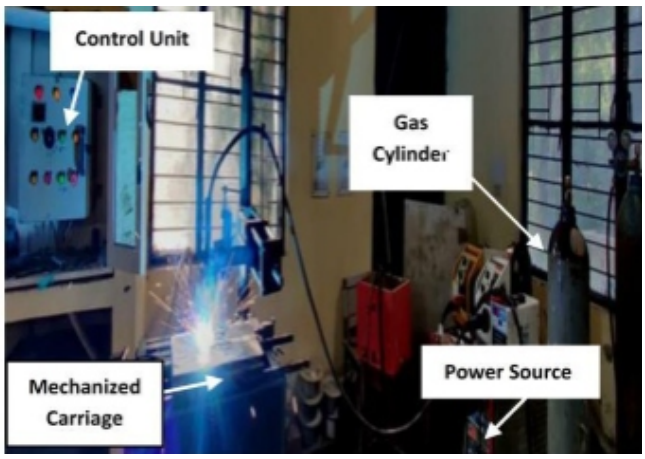

Fig 2: The set-up

III. PLAN OF INVESTIGATION

The research work was planned to be carried out in the following steps:

1) Input parameters
2) Determination of working limits of parameters
3) Generating the matrix using design expert software
4) Experimentation
5) Generation of the mathematical model
6) Examining the adequacy of the generated model
7) Analysis of the result

3.1. Input parameters

Based on previous experience, literature survey and some initial test runs, five independent controllable input parameters were deduced namely "wire feed rate (m/min)", "welding speed (cm/min)", "voltage (V)", "nozzle to plate distance (mm)" and "torch angle (degree)" which had overwhelming effect on angular distortion [1, 8 -14].

3.2. Determination of working limits of parameters

Several test runs were conducted on 200 x 150 x 6 mm plates keeping in consideration the independent input parameters. The working range of each parameter was divided into 5 different levels with -2 and +2 being minimum and maximum levels respectively and -1, 0, +1 being intermediate levels as shown in table - 2.

Run	WFR (m/min)	S (cm/min)	V (Volts)	NPD (mm)	θ (°)	Angular Distortion
1	1	1	-1	-1	1	2.50
2	0	-2	0	0	0	2.04
3	-1	-1	1	1	1	1.51
4	1	-1	1	-1	1	1.93
5	-1	-1	-1	-1	1	1.59

Table - 2: Input parameters and their limits

3.3. Generating the matrix using design expert software

Experiments were performed in a methodical manner and the design matrix was formulated by design expert software using the central composite design. The matrix so obtained to cover the single and interactive effects of input variables is illustrated below in table – 3.

Run	WFR (m/min)	S (cm/min)	V (Volts)	NPD (mm)	θ (°)	Angular Distortion
1	1	1	-1	-1	1	2.50
2	0	-2	0	0	0	2.04
3	-1	-1	1	1	1	1.51
4	1	-1	1	-1	1	1.93
5	-1	-1	-1	-1	1	1.59
6	0	0	0	0	2	2.53
7	0	0	0	0	0	3.23
8	0	2	0	0	0	2.83
9	0	0	2	0	0	1.21
10	1	1	-1	1	-1	1.68

11	0	0	0	0	0	3.35
12	0	0	0	0	0	3.17
13	0	0	0	0	0	3.40
14	-2	0	0	0	0	2.13
15	0	0	0	-2	0	2.17
16	2	0	0	0	0	3.20
17	1	1	1	-1	-1	2.07
18	0	0	-2	0	0	0.63
19	0	0	0	0	0	3.11
20	-1	-1	1	-1	-1	2.01
21	1	1	1	1	1	3.49
22	1	-1	1	1	-1	2.15
23	-1	1	-1	-1	-1	1.77
24	0	0	0	0	0	3.29
25	-1	1	1	1	-1	1.95
26	0	0	0	2	0	2.46
27	1	-1	-1	1	1	2.19
28	0	0	0	0	-2	2.27
29	-1	1	1	-1	1	1.48
30	-1	1	-1	1	1	2.18
31	-1	-1	-1	1	-1	1.81
32	1	-1	-1	-1	-1	1.58

Table - 3: Design Matrix

3.4. Experimentation

The number of runs generated by the design matrix were performed in a desultory manner to eliminate any systematic error, if any. For measurement of angular distortion, the workpiece was kept on a surface plate to achieve meticulous results.

3.5. Generation of the mathematical model

Angular distortion can be represented using the response surface function as:

$$Y = f(\alpha, \beta, \gamma, \delta, \varepsilon)$$

The equationgenerated by response function can be expressed in terms of the independent parameters as: $b0 + b1\alpha + b2\beta + b3\gamma + b4\delta + b5\varepsilon + b12\alpha\beta + b13\alpha\gamma + b14\alpha\delta + b15\alpha\varepsilon + b23\beta\gamma + b24\beta\delta + b25\beta\varepsilon + b34\gamma\delta + b35\gamma\varepsilon + b45\delta\varepsilon + b11\alpha2 + b\ 22\beta2 + b33\gamma2 + b44\delta2 + b55\varepsilon2$ where: Here "Y" represents the angular distortion and "α","β","γ","δ" and"ε" are the input parameters which represent "wire feed rate ", "welding speed", "voltage", "NPD" and"torch angle" respectively, b0 is the coefficient of model, b1, b2...bk are the coefficients of linear terms, b12, b13...b(k-1)k are coefficients of interactive terms and b11, b22...bkk are the coefficients of quadratic terms of the regression equation. Actual mathematical model generated by design expert software is given below:

Angular Distortion (AD) = $53.92 + 5.97\alpha + 2.29\beta + 8.58\gamma - 7.21\delta + 0.82\varepsilon - 3.33\alpha\beta - 3.91\alpha\gamma - 4.21\alpha\delta + 0.86\alpha\varepsilon + 0.52\beta\gamma + 2.14\beta\delta - 8.38\beta\varepsilon - 0.61\gamma\delta + 3.63\gamma\varepsilon - 0.62\delta\varepsilon - 1.5\alpha2 - 0.88\beta2 + 0.79\gamma2 + 1.29\delta2 - 3.49\varepsilon2$

3.6. Examining the adequacy of generated model The adequacy of the generated model was analyzed by comparing the calculated F-ratio given by the software and the tabulated value of F-ratio. As the latter value is greater than the former value, the model can be said to be adequate.

In present case the tabulated value of F-ratio at degree of freedom 6 and 5 at a confidence level of 95% is 4.95 which is more than the calculated value of 2.18 indicating that the developed model is adequate. Secondly, the p-value of the developed model is also less than 0.05, confirming the adequacy of the model as depicted below in table - 4.

S. No.	Response Parameter	First order terms		Second order terms		Lack of fit		Error terms		F-ratio	p-value	R^2	Adequacy of the model
		SS	df	SS	df	SS	df	SS	df				
1	Angular distortion	2.67	5	13.03	15	0.15	6	0.06	5	02.18	0.00001	0.9864	Adequate

Table - 4: ANOVA Table

3.7. Analysis of results

The graphical results obtained by the design expert software are depicted in figure 3 – figure 5. These graphs represent the interactive effects of input parameters on AD and are explained in the following section.

3.7.1 Interactive effects of WFR and NPD on AD

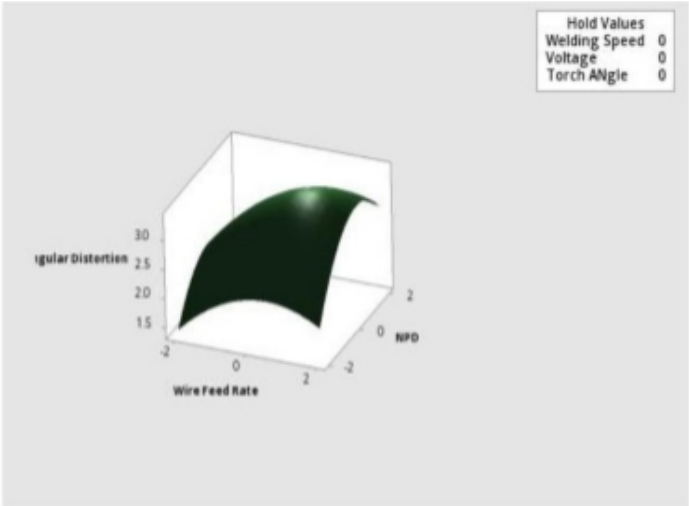

Fig 3: Interactive effects of WFR and NPD on AD

The interactive effects of WFR and NPD on AD are illustrated in figure 3 above. It is ostensible that withboth parametersAD increased. With increase in WFR, the heat input augmented which caused deeper penetration of heat causing more AD. Similarly, with the increase in NPD the resistive heating of filler wire and spread of arc increased over the weld plates causing more AD.

3.7.2 Interactive effects of voltage and WFR on AD

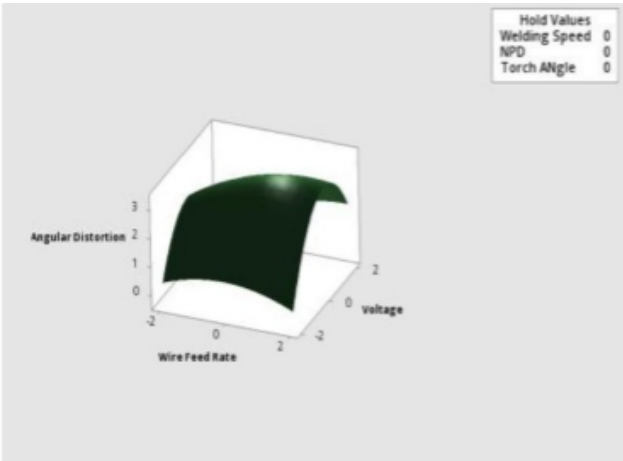

Fig 4: Interactive effects of voltage and WFR on AD

The interactive effects of voltage and WFR on ADare illustrated in the figure 4 above. Due to more heat input into the weld, it is observed the extent of AD augmented. As the voltage increases the AD increasesprimarily and then decreases. The probable reason could be with increase in voltage, results in more heat input and arc spread which increases the AD initially but with further increase in voltage the arc length increased to such a value where radiative heat losses are dominant thereby causing reduction in AD.

3.7.3 Interactive effects of WFR and torch angle on AD

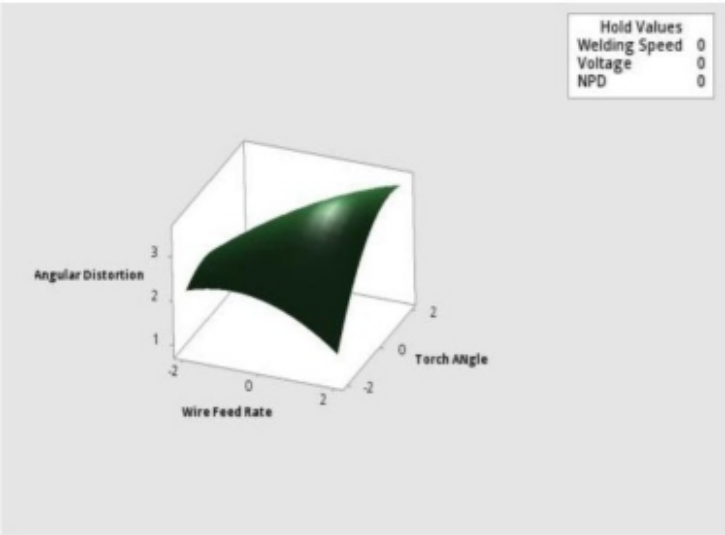

Fig 5: Interactive effects of torch angle and WFR on AD

The interactive effects of WFR and torch angle on AD are illustrated in the 5 above. It is ostensible that both WFR and torch angle have positive effect on AD as maximum angular distortion is obtained at maximum value of WFR and torch angle.

IV. CONCLUSION

The following conclusions are found noteworthy on the basis of investigative work –

1) The (CCFD) and (RSM) are useful in the study and analysis of angular distortion.
2) As voltage increased, angular distortion first increased and then decreased.
3) Welding speed shows a negative influence on AD whereas it was observed to be positive for torch angle.
4) Both NPD and WFR show positive effects on angular distortion.
5) For the minimum value of angular distortion of 0.63°, the optimized values of parameters are: WFR= 0.98 m/min, S = 37 cm/min, V = 22 V, NPD = 15mm and torch angle = 107°.

REFERENCE

[1] Murugan, V.V., Gunaraj, V., "Effects of Process Parameters on Angular Distortion of Gas Metal Arc Welded Structural Steel Plates", American Welding Society and the Welding Research Council, pp. 165-171, November-2005

[2] Vinokurov, V.A., Welding Stresses and Distortion, British Library, 1977

[3] Raju, N., Ravichandran, G., Sudharsanam, V., Easwaran, R., Distortion and its Control in Welding of Stainless Steel Structures, Case Studies Advanced Materials Research, Vol. 794, pp. 358-365, September-2013.

[4] Aggarwal, I., Faujdar, N., Das, A., Khanna, P. "Mathematical Modeling for Predicting Angular Distortion in TIG Welding of Stainless Steel 409L Butt Welds", International Journal of Research in Engineering and Technology, Vol. 07 Issue. 06, pp. 92-97, June-2018.

[5] https://www.metalscope.in/409L-grade.html accessed on 17th March 2020, 13:05hrs
[6] https://www.jindalstainless.com/pdfs/400series.pdf accessed on 17th March 2020, 14:00hrs
[7] Jha, R.K., Kumar, A., Chakraborty, A., Khanna, P., "Effect of Process Parameters on Angular Distortion of GMAW Welded C45 Plates", International Journal of Research in Engineering and Technology, Vol. 07, pp. 168-174, July-2018
[8] Nadzam, J., "Gas Metal Arc Welding, Product and Procedure selection", Lincoln Electric, August 2014.
[9] Ramani, S., Velmurugan, V., "Effect of Process Parameters on Angular distortion of MIG welded AI6061 plates", 26th All India Manufacturing Technology, Design and Research Conference, IIT Guwahati, Assam (AIMTDR-2014).
[10] Gunarajan, V., Murugan, N., "Application of Response surface methodology for predicting weld bead quality in submerged arc welding of pipes", Journal of Materials Processing Technology 88(1-3), pp. 266-275, April-1999.
[11] Adamczuk, P.C, Machado, I.G, Mazzaferro, J.A.E., "Methodology for predicting the angular distortion in multi- pass butt-joint", Welding Journal of Materials Processing Technology, Vol. 240, pp. 305-313, February-2017.
[12] Bergquist, E.L., Huhutala, T., Karlsson, L.," The effect of PURGING GAS on 308L TIG root-pass Ferrite Content" Welding in the world, Springer, Vol. 55, pp. 57-64, 2011.
[13] Mulimbayan, Francis , M., Mena, Manolo , G., "Comparative Study of the Corrosion Behavior of Low-Nickel AISI 202 and Conventional AISI 304 Stainless Steels in Citric Acid using Electrochemical Techniques" Applied Mechanics and Materials, ISSN: 1662-7482, Vol. 835, pp. 131- 135, 2016.
[14] Kim, I.S., Son, J.S., Park, C.E., Kim, I.J., Kim, H.H.," An investigation into an intelligent system for predicting bead geometry in GMA welding process," Journal of Materials Processing Technology, Vol. 159, pp. 113–118, 2005.

Comparative Studies in Minimizing the Corrosion Behavior of AA7075 through Advancedcoating Techniques

[1] S. PREMKUMAR, [2] G. NAVEEN SUBRAMANIAN

[1]Engineer, Department of Corrosion control, quest Global Engg. Services, Pvt. Ltd, Bangalore, India

[2]Engineer, Department of Design, QuEST Global Engg. Services, Pvt. Ltd, Bangalore, India

E-mail: [1]Premkumar.s@quest-global.com, [2]Naveen.Govindaraju@quest-global.com

A B S T R A C T

Aluminium AA7075 material has found to have a widespread application in aerospace and automotive industry owing to its better mechanical properties. Localized Corrosion was found to have a major issue, occurring in AA7075 material which limits its application in certain areas. Lot of research work is ongoing in enhancing the corrosion resistance of the material. Nano powder based Metal coating has been found to be more effective in reducing metal affinity towards corrosion and acts as a protective surface to the substrate against the corrosion. Collective studies related to different coating techniques performed on AA7075 is limited. Hence in this review paper, comparative studies related to ceramic Nano composites and polymer based coating on AA7075by Plasma Electrolytic Oxidation (PEO)and chemical synthesis process are discussed. Also the performance of coating are explained in-order to understand its effectiveness. Finally, the corrosion behavior of above coatings, fabricated on AA7075 material are studied using Potentio-dynamic polarization (PDP) techniques and the surface morphology of the material was studied through microscope and SEM analysis.

Keywords - AA7075, Ceramic Nanometal Coating, Polymer Coating, PEO, Chemical Synthesis Method, PDP, Coating Effectiveness.

I. INTRODUCTION

The applications of AA7075 aluminum alloy as a structural materials in sectors like aircraft, automobiles, and spacecraft elements is increasing because of its desirable strength to weight characteristics. Structural weight reduction enhances the payload capacity of the aircraft as well as better fuel consumption which results in optimized performance of the spacecraft's [1-3].But due to the presence of intermetallics in its microstructure which are formed during alloying process, they are highly susceptible to localized corrosion[4]. Hence to avoid metallic corrosion, various coatings are performed on AA7075 based on its application and work environment.

Radiation protection and thermal control with desired absorptance and emittance values are the important properties that are required in the spacecraft components. In electronic house packages for thermal control applications, black corrosion resistant coating with the high emittance are the requirement for internal spacecraft components [5].Shrestha et al. [6] found better thermo-optical properties along with acceptable corrosion resistance on high strength aluminum alloys AA7075 & AA2219 with black PEO coatings.

Also the European Space Agency (ESA) extensively studied the Gray black PEO coatings on aluminum alloys (AA2219 and AA7075Z) as thermal-control coatings for spacecraft material applications Conventionally, Chromate conversion based coatings are used widely to avoid corrosion. But chromate coatings have toxic hexavalent chromium and because of this, chromate-free coatings are increasingly preferred with better corrosion protection properties. Hence for corrosion protection coatings,

polymers have been introduced in painting formulations. For better corrosion protection Polyaniline (PANI) has been reported as a coating, because of its redox properties Mirmohseni and Oladegaragoze [7] investigated PANI coatings on iron by chemically synthesized and deposited technique and their results revealed that the PANI coating promoted low porosity and enhanced corrosion protection due to the formation of an oxide passive layer on the substrate [8].

For valve metals (Al, Mg, Ti and Zr and its alloys) undergoing high wear and abrasion, Plasma electrolytic oxidation (PEO) considered to be widely used coating technologies [9–12].

From the above literature review, it is clearly seen that, various coatings were performed on AA7075 through PEO and chemical synthesis techniques to enhance the corrosion resistance of the base metal. But very limited, comparative studies are available. Hence in this present review work, detailed comparison of polymer and ceramic based coatings performed on AA7075 was studied.

II. POLYANILINE/POLYVINYL CHLORIDE BLENDED COATINGS PERFORMED ON AA7075 BY CHEMICAL SYNTHESIS METHOD.

Rafael Marinho et.al [13] chemically synthesized blended Polyaniline and Polyvinyl chloride coatings for the corrosion protection of AA7075 aluminum alloyin 3.5% NaCl solution with(thicknesses 5 - 30 µm) were used. In their investigation when examinedby electron microscopy, it is found that PVC predominated at the surface by forming well-defined structure, and constituted bulkmatrix. PANI at the substrate/coating interface formed agglomerates within the bulk and concentrated in a layer.

Surface morphologies, cross-section analysis. PANI is used as a corrosion protection coating and the surface morphology represents presence of intrinsic pores or cracks in the coating. This affects the performance for long exposure times. Hence to avoid this and to improve the adhesion, structureand morphology modified PANI-based coatings are fabricated. PANI/PVC blends provided defect-free surface, as PVC acts as a second component that can fill out the structure which improves the physical barrier effect by decreasing the porosity and water uptake.The surface roughness of the coated specimen was analyzed by atomic force microscope (AFM) and the results are represented from figures 1 a-d.Figure 1bdisplays Nano scale holes which that can evolve to pores. The morphology of the PANI/PVC 1/1 coating (Figure 1d) is similar to that of PVC, with deflections that are more pronounced and display a gravel like texture.

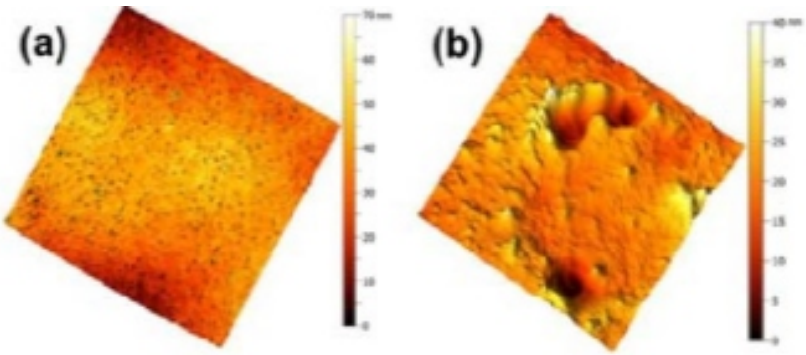

(a) PANI (90 µm x 90 µm) (b) PANI (3.2 µm x 3.2 µm)

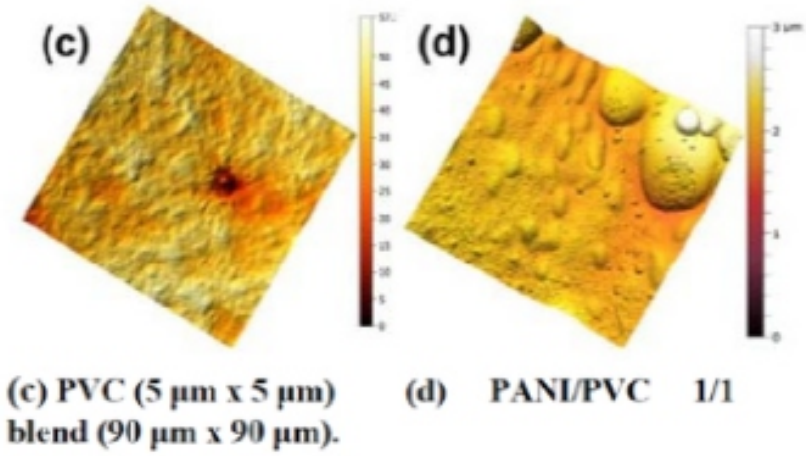

Figure 1 a-d. AFM images of PANI, PVC, and PANI/PVC blend at several magnifications.

Coating Performance: The corrosion protection for AA7075-T6 aluminum alloy is largely influenced by the roughness and thickness of the coating material. PANI has low water intake capability when the coating was smooth. On the other hand, coating with high thickness provides high roughness and reduces the corrosion protection behavior. Hence, more than the thickness, the performance was linked to the roughness and morphology of the coatings. The thick coatings have lower roughness values which also decreases the superficial area of electrolyte exposure.

III. CERAMIC NANO COMPOSITE COATINGS TREATED AA7075 BY PLASMA ELECTROLYTIC OXIDATION (PEO) METHOD.

Ceramic nanoparticles (α-Al2O3 and m-ZrO2) through plasma electrolytic oxidation method were fabricated on AA7075in silicate + KOH electrolyte. It is found that the hard α-Al2O3 incorporated coating shows improved corrosion resistance than m-ZrO2 incorporated coating. This is due to the presence of hard α-Al_2O_3 in the coating structure with higher thickness. Henceforth, the corrosion resistance of the α-Al_2O_3 has improved.In- order to enhance the corrosion resistance, hydrophobic surfaces were made on PEO treated α-Al_2O_3 and m-ZrO2 coatedAA7075 by stearic acid and myristic acid.

Surface morphology study by SEM analysis: SEM microstructure reveals the closed pore morphology with leaf-shaped ridges formed on the surface of sample. However, pedal like features was observed in the surface SEM microstructure of stearic acid modified PEO treated sample AA-S as shown in fig 2(a-b).

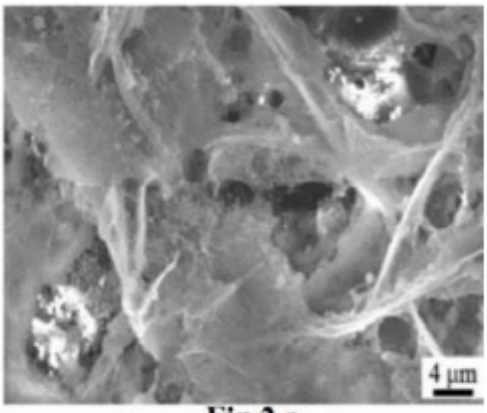

Fig 2.a

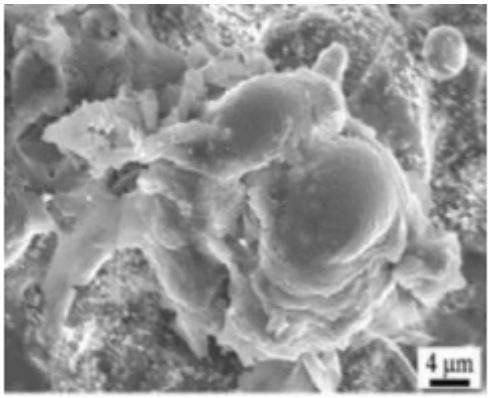

Fig 2.b

There is no discontinuity at the interface as the PEO- coated samples show better adhesion to the substrate. Although PEO coatings show porous microstructure, there is no evident of thickness pores,this implies that the poresare present on the surface of the coatings are shallow and partially filled with coating materials and nanoparticles. The PEO treated samples thicknesses ofA, AA and AZ are 20±1 µm, 26±1 µm and 24±1 µm, respectively

.

3.1 Comparative analysis of Electro chemical study (Potentio-dynamic Polarization) results:

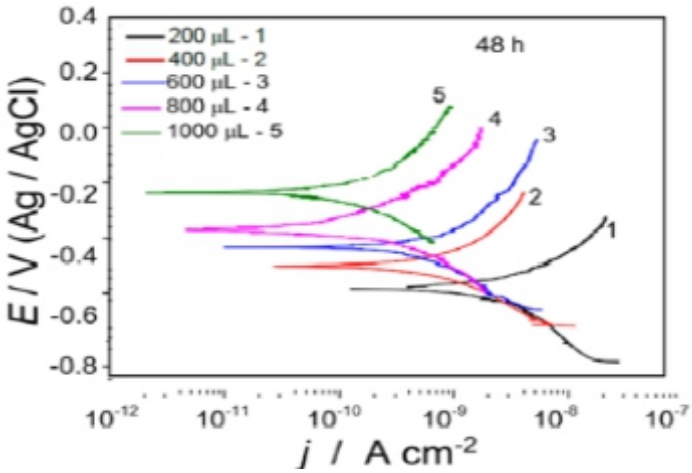

Fig3. a. PANI/PVC PDP results

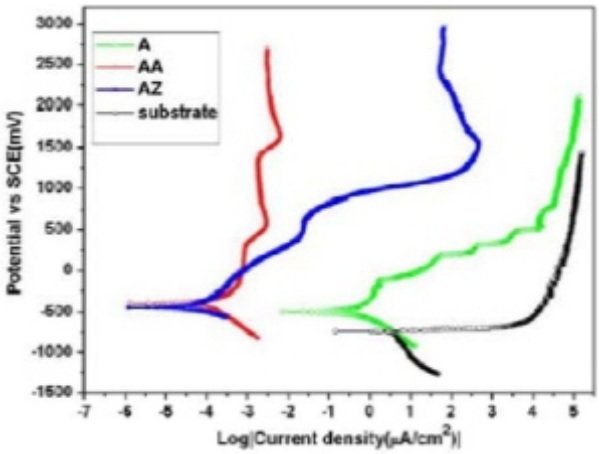

Fig3. b. PEO treated samples A, AA and AZ PDP results.

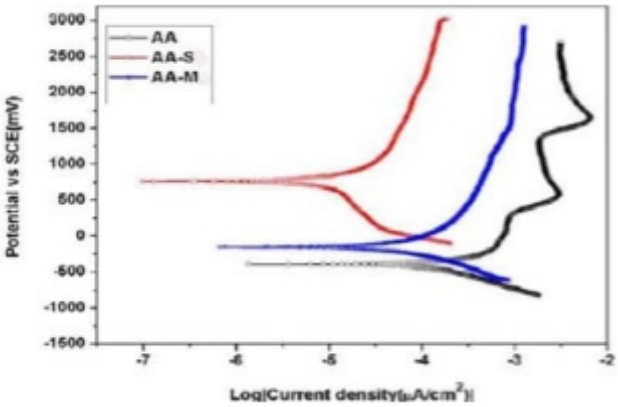

Fig 3.c. PDP curves for samples AA, AA-S and AA-M in 3.5 wt% NaCl

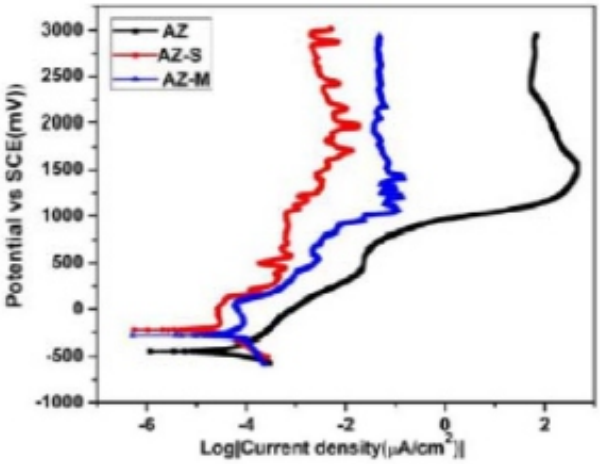

Fig 3.d.PDP curves for samples AZ, AZ-S and AZ-M in 3.5 wt% NaCl.

From the Polarization measurements results, thecorrosion current densities Icorr for the PANI/PVC(fig 3.a)polymer coatingsexhibited lower value when compared to that of same material, which indicateslow susceptibilities to corrosion. The increased corrosion protection performance relative to comparable pure PANI coating of comparable thickness as proven by the electrochemical measurements.

On the other hand, corrosion resistance of the nanoparticle incorporated PEO coatings significantly improved by the hydrophobic treatments.The sample A, PEO treated with KOH and silicate electrolyte solution, sample AA with PEO treated α-Al2O3 nanoparticles and AZ, PEO treated m-ZrO2 nanoparticles. Correspondingly AA-S and AA-M relates to stearic acid modified PEO treated α-Al2O3 and AZ-S and AZ-M represents myristic acid modified PEO treated m-ZrO2 nanoparticles.

The stearic acid modified PEO treated α- Al2O3sample exhibited highest Ecorr and lowest icorr values(fig 3.d). Which provided sealed pore morphology and enhanced the corrosion resistance of the sample. Also, polymer based coatings has greater Ecorr value, which directly indicates the much high corrosion resistance of the material when compared with ceramic based coatings.

IV. DISCUSSION

Chemical synthesized PANI processed coatings has the presence of pores, that allows water uptake, this makes the coating structure undergoes expansion and relaxation and worsens the coating strength, if

has long exposure times. Hence in this situation, relatively quickcorrosion process occurs and there is not appropriate time for PANI to support the formation of a passive and stable layer of metallic oxide.Electrochemical tests provenhigh resistance to water uptake, low susceptibility to corrosion,good performance,and low corrosion current densities over 15 days of exposure to saline solution. Polymers possess good adhesion and has the advantage of easy processability characteristics.[15-18].

Comparatively in ceramic coating, due to the incorporation of nanoparticles into the coating,Grain level uniform distribution of coating material with the substrate is formed, increases the thickness, and consequently for the current higher discharge energy is required to pass through it. Because of the higher discharge energy, relatively bigger pores and thick pancake like features are created on its surface. It is to be noted that discharge pores generally help the oxygen evolution to escape its way through the coating and may help to form the stable growth of PEO coating without oxygen entrapment. The stearic acid modified Al2o3PEO coating showed excellent corrosion resistance.Stearic acid treatment seal the micro pores which are formed and hence the water droplet is not quickly penetrating the sample and exhibits better corrosion resistance behavior.Two layer structures namely, outer porous layer and inner dense layer was exhibited byPEO coated samples [19].Better mechanical interlocking was provided by the outer porous layer which improves the adhesion of organic or polymeric topcoats. In contrast, using chemical synthesis approach large-scale production is made possible [20].

On comparing both the polymer and ceramic coating, their selection for corrosion protection depends on few factors, like operating temperature and service environments, for higher temperatures ceramic coatings are used. Polymer based coating are less in cost when compared with Nano sized ceramics and offers excellent corrosion protection as long as the coating was smooth and intact. But for applications involving wear, ceramic Nano particles withstand the environmental abrasion and provide protection to the substrate.

V. CONCLUSION

1. A detailed comparison between ceramic based Nano coatings and polymer based coating were made and their corrosion behaviors are studied.
2. Electrochemical analyses showed that there is enhanced protection using blends when compared to pure PANI coatings with reduced porosity
3. The blend showed a distribution of PVC and PANI domains that contributed to its better protection performance.
4. The PEO treatment can be employed to fabricate thick ceramic coatings with highcorrosion resistance, higher hardness good thermal stability and with better wear resistance property.
5. In ceramic coatings, the corrosion resistance of α-Al2O3 incorporated PEO coating is significantly improved by hydrophobic treatments.

REFERENCE

[1] *A.K. Mukhopadhyay, A.K. Sharma, Influence of Fe-bearing particles and nature of electrolyte on the hard anodizing behaviour of AA 7075 extrusion products, Surf. Coat. Technol. 92 (1997) 212–220.*

[2] *R. Uma Rani, A.K. Sharma, S.M. Mayanna, H. Bhojraj, D.R. Bhandari, Black permanganate conversion coatings on aluminium alloys for thermal control of spacecraft, Surf. Eng. 21 (2005) 198–203.*

[3] *I.J. Polmear, Light Alloys: From Traditional Alloys to Nano crystals, fourth ed., Elsevier Butterworth-Heinemann, United Kingdom, 2006.*

[4] *N. Birbilis, R.G. Buchheit, Electrochemical characteristics of intermetallic phases in aluminum alloys, J. Electrochem. Soc. 152 (2005) B140-B151.*

[5] *A.K. Sharma, Surface engineering for thermal control of spacecraft, Surf. Eng. 21 (2005) 249–253.*

[6] S. Shrestha, P. Shashkov, B. D. Dunn, Microstructural and thermo-optical properties of black Keronite PEO coating on aluminium alloy AA7075 for spacecraft materials applications, Proc. '10th Intl. Symposium on Materials in a Space Environment, Collioure, France. 2006.

[7] A. Mirmohseni, A. Oladegaragoze, Anti-corrosive properties of polyaniline coating on iron, Synthetic Metals, 114 (2000) 105-108.

[8] Y.Y. Zhao, Z.M. Zhang, L.M. Yu, Corrosion protection of carbon steel by electrospun film containing polyaniline microfibers, Reactive & Functional Polymers, 102 (2016) 20- 26.

[9] A.L. Yerokhin, A. Shatrov, V. Samsonov, P. Shashkov, A. Pilkington, A. Leyland, A. Matthews, Oxide ceramic coatings on aluminium alloys produced by a pulsed bipolar plasma electrolytic oxidation process, Surf. Coat. Technol. 199 (2005) 150–157.

[10] S.L. Aktuğa, S. Durdua, I. Kutbaya, M. Ustaa, Effect of Na2SiO3•5H2O concentration on microstructure and mechanical properties of plasma electrolytic oxide coatings on AZ31 Mg alloy produced by twin roll casting, Ceram. Int. 42 (2016) 1246–1253.

[11] M. Sandhyarani, T. Prasadrao, N. Rameshbabu, Role of electrolyte composition on structural, morphological and in- vitro biological properties of plasma electrolytic oxidation films formed on zirconium, Appl. Surf. Sci. 317 (2014) 198– 209.

[12] S. Hariprasad, M. Ashfaq, T. Arunnellaiappan, M. Harilal, Role of electrolyte additives on in-vitro corrosion behavior of DC plasma electrolytic oxidization coatings formed on Cp-Ti, Surf. Coat. Technol. 292 (2016) 20–29.

[13] Bandeira RM, van Drunen J, de Souza Ferreira FA, Filho UPR, Tremiliosi-Filho G, Chemically synthesized polyaniline/polyvinyl chloride blended coatings for the corrosion protection of AA7075 aluminum alloy, Corrosion Science (2010), https://doi.org/10.1016/j.corsci.2018.04.031

[14] Arunnellaiappan, T., Ceramics International (2017),http://dx.doi.org/10.1016/j.ceramint.2017.10.014

[15] N. Ahmad, A.G. MacDiarmid, Inhibition of corrosion of steels with the exploitation of conducting polymers, Synthetic Metals, 78 (1996) 103-110.

[16] G.M. Spinks, A.J. Dominis, G.G. Wallace, D.E. Tallman, Electroactive conducting polymers for corrosion control - Part 2. Ferrous metals, Journal of Solid State Electrochemistry, 6 (2002) 85-100.

[17] P.J. Kinlen, D.C. Silverman, C.R. Jeffreys, Corrosion protection using polyaniline coating formulations, Synthetic Metals, 85 (1997) 1327-1332.

[18] M. Kraljic, Z. Mandic, L. Duic, Inhibition of steel corrosion by polyaniline coatings, Corrosion Science, 45 (2003) 181- 198.

[19] T.S.N. Sankara Narayanan, I.S. Park, M.H. Lee, Strategies to improve the corrosion resistance of micro arc oxidation (MAO) coated magnesium alloys for degradable implants: prospects and challenges, Prog. Mater. Sci. 60 (2014) 1–71.

[20] N. Ahmad, A.G. MacDiarmid, Inhibition of corrosion of steels with the exploitation of conducting polymers, Synthetic Metals, 78 (1996) 103-110.

Instructions for Authors

Essentials for Publishing in this Journal

1 Submitted articles should not have been previously published or be currently under consideration for publication elsewhere.

2 Conference papers may only be submitted if the paper has been completely re-written (taken to mean more than 50%) and the author has cleared any necessary permission with the copyright owner if it has been previously copyrighted.

3 All our articles are refereed through a double-blind process.

4 All authors must declare they have read and agreed to the content of the submitted article and must sign a declaration correspond to the originality of the article.

Submission Process

All articles for this journal must be submitted using our online submissions system. http://enrichedpub.com/ . Please use the Submit Your Article link in the Author Service area.

Manuscript Guidelines

The instructions to authors about the article preparation for publication in the Manuscripts are submitted online, through the e-Ur (Electronic editing) system, developed by **Enriched Publications Pvt. Ltd**. The article should contain the abstract with keywords, introduction, body, conclusion, references and the summary in English language (without heading and subheading enumeration). The article length should not exceed 16 pages of A4 paper format.

Title

The title should be informative. It is in both Journal's and author's best interest to use terms suitable. For indexing and word search. If there are no such terms in the title, the author is strongly advised to add a subtitle. The title should be given in English as well. The titles precede the abstract and the summary in an appropriate language.

Letterhead Title

The letterhead title is given at a top of each page for easier identification of article copies in an Electronic form in particular. It contains the author's surname and first name initial .article title, journal title and collation (year, volume, and issue, first and last page). The journal and article titles can be given in a shortened form.

Author's Name

Full name(s) of author(s) should be used. It is advisable to give the middle initial. Names are given in their original form.

Contact Details

The postal address or the e-mail address of the author (usually of the first one if there are more Authors) is given in the footnote at the bottom of the first page.

Type of Articles

Classification of articles is a duty of the editorial staff and is of special importance. Referees and the members of the editorial staff, or section editors, can propose a category, but the editor-in-chief has the sole responsibility for their classification. Journal articles are classified as follows:

Scientific articles:

1. Original scientific paper (giving the previously unpublished results of the author's own research based on management methods).
2. Survey paper (giving an original, detailed and critical view of a research problem or an area to which the author has made a contribution visible through his self-citation);
3. Short or preliminary communication (original management paper of full format but of a smaller extent or of a preliminary character);
4. Scientific critique or forum (discussion on a particular scientific topic, based exclusively on management argumentation) and commentaries. Exceptionally, in particular areas, a scientific paper in the Journal can be in a form of a monograph or a critical edition of scientific data (historical, archival, lexicographic, bibliographic, data survey, etc.) which were unknown or hardly accessible for scientific research.

Professional articles:

1. Professional paper (contribution offering experience useful for improvement of professional practice but not necessarily based on scientific methods);
2. Informative contribution (editorial, commentary, etc.);
3. Review (of a book, software, case study, scientific event, etc.)

Language

The article should be in English. The grammar and style of the article should be of good quality. The systematized text should be without abbreviations (except standard ones). All measurements must be in SI units. The sequence of formulae is denoted in Arabic numerals in parentheses on the right-hand side.

Abstract and Summary

An abstract is a concise informative presentation of the article content for fast and accurate Evaluation of its relevance. It is both in the Editorial Office's and the author's best interest for an abstract to contain terms often used for indexing and article search. The abstract describes the purpose of the study and the methods, outlines the findings and state the conclusions. A 100- to 250-Word abstract should be placed between the title and the keywords with the body text to follow. Besides an abstract are advised to have a summary in English, at the end of the article, after the Reference list. The summary should be structured and long up to 1/10 of the article length (it is more extensive than the abstract).

Keywords

Keywords are terms or phrases showing adequately the article content for indexing and search purposes. They should be allocated heaving in mind widely accepted international sources (index, dictionary or thesaurus), such as the Web of Science keyword list for science in general. The higher their usage frequency is the better. Up to 10 keywords immediately follow the abstract and the summary, in respective languages.

Acknowledgements

The name and the number of the project or programmed within which the article was realized is given in a separate note at the bottom of the first page together with the name of the institution which financially supported the project or programmed.

Tables and Illustrations

All the captions should be in the original language as well as in English, together with the texts in illustrations if possible. Tables are typed in the same style as the text and are denoted by numerals at the top. Photographs and drawings, placed appropriately in the text, should be clear, precise and suitable for reproduction. Drawings should be created in Word or Corel.

Citation in the Text

Citation in the text must be uniform. When citing references in the text, use the reference number set in square brackets from the Reference list at the end of the article.

Footnotes

Footnotes are given at the bottom of the page with the text they refer to. They can contain less relevant details, additional explanations or used sources (e.g. scientific material, manuals). They cannot replace the cited literature.
The article should be accompanied with a cover letter with the information about the author(s): surname, middle initial, first name, and citizen personal number, rank, title, e-mail address, and affiliation address, home address including municipality, phone number in the office and at home (or a mobile phone number). The cover letter should state the type of the article and tell which illustrations are original and which are not.

Address of the Editorial Office:

Enriched Publications Pvt. Ltd.
S-9,IInd FLOOR, MLU POCKET,
MANISH ABHINAV PLAZA-II, ABOVE FEDERAL BANK,
PLOT NO-5, SECTOR -5, DWARKA, NEW DELHI, INDIA-110075,
PHONE: - + (91)-(11)-45525005